Neurobiology of Disease 155 (2021) 105391

Contents lists available at ScienceDirect

Neurobiology of Disease

journal homepage: www.elsevier.com/locate/ynbdi

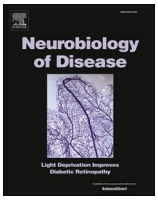

Modeling chemotherapy induced neurotoxicity with human induced pluripotent stem cell (iPSC) -derived sensory neurons

Christian Schinke [a,b], Valeria Fernandez Vallone [c], Andranik Ivanov [d], Yangfan Peng [a,e], Péter Körtvelyessy [a,f,g], Luca Nolte [a], Petra Huehnchen [a,b,h], Dieter Beule [d,i], Harald Stachelscheid [c], Wolfgang Boehmerle [a,b,h,1,*], Matthias Endres [a,b,h,j,k,l,1]

[a] Charité - Universitätsmedizin Berlin, corporate member of Freie Universität Berlin and Humboldt-Universität zu Berlin, Klinik und Hochschulambulanz für Neurologie, Charitéplatz 1, 10117 Berlin, Germany
[b] Berlin Institute of Health at Charité, Universitätsmedizin Berlin, Anna-Louisa-Karsch Straße 2, 10178 Berlin, Germany
[c] Berlin Institute of Health at Charité – Universitätsmedizin Berlin, Stem Cell Core Facility, Augustenburger Platz 1, 13353 Berlin, Germany
[d] Berlin Institute of Health at Charité – Universitätsmedizin Berlin, Core Unit Bioinformatics, Charitéplatz 1, 10117 Berlin, Germany
[e] Charité - Universitätsmedizin Berlin, corporate member of Freie Universität Berlin, Humboldt-Universität zu Berlin, Institut für Neurophysiologie, Charitéplatz 1, 10117 Berlin, Germany
[f] Charité – Universitätsmedizin Berlin, corporate member of Freie Universität Berlin and Humboldt-Universität zu Berlin, Department of Neuropathology, Charitéplatz 1, 10117 Berlin, Germany
[g] German Center for Neurodegenerative Diseases, 39120 Magdeburg, Germany
[h] Charité - Universitätsmedizin Berlin, corporate member of Freie Universität Berlin, Humboldt-Universität zu Berlin, NeuroCure Cluster of Excellence, Charitéplatz 1, 10117 Berlin, Germany
[i] Max-Delbrueck Center for Molecular Medicine, 13125 Berlin, Germany
[j] Charité - Universitätsmedizin Berlin, corporate member of Freie Universität Berlin, Humboldt-Universität zu Berlin, Center for Stroke Research Berlin, Charitéplatz 1, 10117 Berlin, Germany
[k] German Center for Neurodegenerative Diseases (DZNE), partner site Berlin, Germany
[l] German Center for Cardiovascular Research (DZHK), partner site Berlin, Germany

ARTICLE INFO

Keywords:
Induced pluripotent stem cell derived sensory neurons (iPSC-DSN)
Chemotherapy induced neuropathy
3R
Replacement
Transcriptome
Lithium

ABSTRACT

Chemotherapy-induced peripheral neuropathy (CIPN) is a frequent, potentially irreversible adverse effect of cytotoxic chemotherapy often leading to a reduction or discontinuation of treatment which negatively impacts patients' prognosis. To date, however, neither predictive biomarkers nor preventive treatments for CIPN are available, which is partially due to a lack of suitable experimental models. We therefore aimed to evaluate whether sensory neurons derived from induced pluripotent stem cells (iPSC-DSN) can serve as human disease model system for CIPN. Treatment of iPSC-DSN for 24 h with the neurotoxic drugs paclitaxel, bortezomib, vincristine and cisplatin led to axonal blebbing and a dose dependent decline of cell viability in clinically relevant IC_{50} ranges, which was not observed for the non-neurotoxic compounds doxorubicin and 5-fluorouracil. Paclitaxel treatment effects were less pronounced after 24 h but prominent when treatment was applied for 72 h. Global transcriptome analyses performed at 24 h, i.e. *before* paclitaxel-induced cell death occurred, revealed the differential expression of genes of neuronal injury, cellular stress response, and sterol pathways. We further evaluated if known neuroprotective strategies can be reproduced in iPSC-DSN and observed protective effects of lithium replicating findings from rodent dorsal root ganglia cells. Comparing sensory neurons derived from two different healthy donors, we found preliminary evidence that these cell lines react differentially to neurotoxic drugs as expected from the variable presentation of CIPN in patients. In conclusion, iPSC-DSN are a promising platform to study the pathogenesis of CIPN and to evaluate neuroprotective treatment strategies. In the future,

Abbreviations: BTZ, bortezomib; CIPN, chemotherapy-induced peripheral neuropathy; CIS, cisplatin; CGRP, calcitonine gene related peptide; CTX, chemotherapy; FDA, fluoresceine diaceteate; IC_{50}, half-maximal inhibitory concentration; iPSC-DSN, induced pluripotent stem cell-derived sensory neurons; PTX, paclitaxel; TPM, transcripts per kilobase million; TRPA1, transient receptor potential cation channel, subfamily A member 1; TRPM8, transient receptor potential cation channel subfamily M member 8; VIN, vincristine.

* Corresponding author at: Klinik und Hochschulambulanz für Neurologie, Charité Universitätsmedizin Berlin, Germany.
E-mail address: wolfgang.boehmerle@charite.de (W. Boehmerle).

[1] Indicates equal contribution.

https://doi.org/10.1016/j.nbd.2021.105391
Received 23 March 2021; Received in revised form 6 May 2021; Accepted 7 May 2021
Available online 11 May 2021

the application of patient-specific iPSC-DSN could open new avenues for personalized medicine with individual risk prediction, choice of chemotherapeutic compounds and preventive treatments.

1. Introduction

Chemotherapy-induced peripheral neuropathy (CIPN) is one of the most common side effects of cytotoxic chemotherapy and is clinically characterized by altered sensation, sensory loss and neuropathic pain. CIPN not only further increases the burden of disease but often necessitates reduction or even discontinuation of chemotherapy and thereby limits the patients' prognosis (Boehmerle et al., 2014; Knauss et al., 2019). About two thirds of patients who undergo cytotoxic treatment develop CIPN (Boehmerle et al., 2014; Seretny et al., 2014), and therapeutic options are currently limited to termination of treatment, dose reductions or often ineffective symptomatic treatment (Smith et al., 2013). Despite some genome wide association studies which suggest candidate single nucleotide polymorphisms to be associated with CIPN (Mahmoudpour et al., 2018), it is not yet possible to predict which patient will develop adverse effects and to what extent. Likewise, biomarkers as well as clinically tested preventive strategies in patients are presently not available. Even though targeted therapies with antibodies or genetic approaches continue to transform modern cancer treatment, 'classic' cytotoxic treatments still remain a pivotal part of routine cancer therapy for the foreseeable future (reviewed by Boehmerle et al. (2014), Knauss et al. (2019)). With an increasing number of cancer survivors, irreversible neurologic sequelae of chemotherapy such as CIPN present a major unmet medical need. The incomplete understanding of the underlying pathophysiology of CIPN is partly due to a lack of adequate human disease models. With the generation of induced pluripotent stem cells (iPSC) from adult human cells (Takahashi et al., 2007; Hennig et al., 2019) and their further differentiation into cell types such as iPSC-derived sensory neurons (Chambers et al., 2012; Schwartzentruber et al., 2018) or cardiomyocytes (Burridge et al., 2014), otherwise inaccessible human tissue has become available to model human diseases in vitro. Previous studies demonstrated neurotoxic effects of antineoplastic therapy on commercially available neurons of the peripheral (Wing et al., 2017) and central (Wheeler et al., 2015) human nervous system and in neurons converted from peripheral-blood-derived neural progenitors (Vojnits et al., 2019). Previously, iPSC-derived cardiomyocytes were shown to reflect patients' individual susceptibility to doxorubicin-induced cardiomyopathy, indicating iPSC-based models to be a promising platform to study the effects of chemotherapy-induced toxicity in a patient-specific human disease model (Burridge et al., 2016).

In the present study, we tested the suitability of iPSC-derived sensory neurons (iPSC-DSN) as a human cellular disease model of chemotherapy-induced neurotoxicity. We were interested whether neurotoxic chemotherapy in clinically relevant steady state concentrations affects cell viability and axonal integrity in iPSC-DSN, and if these effects are substance specific compared with cytotoxic drugs which typically do not cause neuropathy. Using paclitaxel as a prototype of a neurotoxic chemotherapy, we analyzed the global transcriptome of sensory neurons *before* apparent cell death occurs, and evaluated if the previously reported neuroprotectant lithium (Mo et al., 2012) can replicate neuroprotective effects in the human iPSC-DSN model. We further tested if iPSC-DSN derived from two distinct donors may react differentially upon neurotoxic chemotherapy as observed from differential CIPN susceptibilities known from humans (Mahmoudpour et al., 2018).

2. Material and methods

A detailed description is found in the Supplemental Material.

2.1. iPSC lines

iPSC-derived sensory neurons were differentiated from two established stem cell lines (s.c. BIHi005-A https://hpscreg.eu/cell-line/BIHi005-A and BIHi004-B https://hpscreg.eu/cell-line/BIHi004-B, Berlin Institute of Health Stem Cell Core Facility). These lines were derived by reprogramming of human dermal fibroblasts using Sendai viral vectors as described previously (Hennig et al., 2019; Fusaki et al., 2009). Cells were maintained on growth factor reduced Geltrex (Gibco) in E8 media, which was exchanged daily. Cells were enzymatically clump-passaged every 2–4 days when >70% confluency was reached using EDTA (UltraPure™ 0.5 M EDTA, Thermo Fisher).

2.2. Sensory neuron differentiation and maintenance

The s.c. *P2 protocol* by Schwartzentruber et al. (2018) was applied for hiPSC differentiation (Fig. 1 A). In brief, confluent clump-passaged iPS-cells were single cell seeded at a density between 200.000 and 400.000/well into 6-well plates (Falcon) coated with growth factor reduced Geltrex (Gibco) and cultivated in E8 media until 70–80% confluency was achieved, which usually required 48 to 72 h. *On day 0*, neural induction was commenced by replacing E8 media with Knockout Serum Replacement Media (500 ml DMEM-KO [Gibco] supplemented with 130 ml CTS KnockOut SR XenoFree Medium (Gibco), 1× MEM-Non-essential Amino Acid Solution (Sigma), 1× Glutamax (Gibco) and 0.01 mM β-Mercapto-ethanol (Gibco) containing the two small molecule inhibitors '2i': 100 nM LDN-193189 (Sigma) and 10 μM SB-431542 (Peprotech) to drive neuroectoderm differentiation. *On day 3*, '3i' consisting of 3 μM CHIR99021 (Sigma), 10 μM DAPT (Sigma) and 10 μM SU5402 (Sigma) were added to promote neural crest specification. *On day 4*, N2B27 media (500 ml Neurobasal-Medium [Gibco], 5 ml of N-2 (100×) supplement [Gibco], 10 ml of B27-supplement (50×) without Vitamin A [Gibco], 1× Glutamax and 0.01 mM β-Mercapto-ethanol [Sigma]) was progressively phased in. From day 7 onwards, '2i' addition was ceased but '3i' continued to be added until Day 11 (Fig. 1 A). On day 11, iPSC-DSN were reseeded or cryopreserved according to the protocols of Schwartzentruber et al. (2018) and Stacey et al. (2018), respectively, and as described in detail in *Suppl. methods*. On day 14, cells were treated with 1 μg/ml Mitomycin C (Sigma) for 2 h to eliminate few dividing non-neuronal cells. iPSC-DSN were maturated for at least four more weeks, and half media change was performed every 3–4 days with N2B27 supplemented with BDNF, GDNF, βNGF and NT3 (all at 25 ng/ml, Peprotech). For this study, 12 independent differentiations were performed, carried out by the same experimenter.

2.3. Whole cell patch-clamp

Whole cell patch-clamp experiments were performed between maturation day 33 and 37 on a multi-neuron patch-clamp setup (Peng et al., 2019; Peng et al., 2017) with extra- and intracellular solutions according to Namer et al. (2019). Glass pipettes were pulled from borosilicate glass capillaries (2 mm outer/1 mm inner diameter; Hilgenberg) on a horizontal puller (P-97, Sutter Instrument Company) with a pipette resistance of 5–8 MΩ. Recordings were performed in a submerged recording chamber containing a geltrex-coated coverslip and perfused with an extracellular solution at room temperature containing in mM: 140 NaCl, 3 KCl, 1 $CaCl_2$,1 $MgCl_2$, 10 HEPES and 20 D-Glucose (pH 7.4) (Namer et al., 2019). Glass pipettes were filled with intracellular solution containing in mM: 4 NaCl, 135 K-gluconate, 3 MgCl2, 5 EGTA, 5 HEPES, 2 Na2-ATP and 0.3 Na3-GTP (pH 7.25) (Namer et al., 2019). Cells were visualized by an infrared differential interference

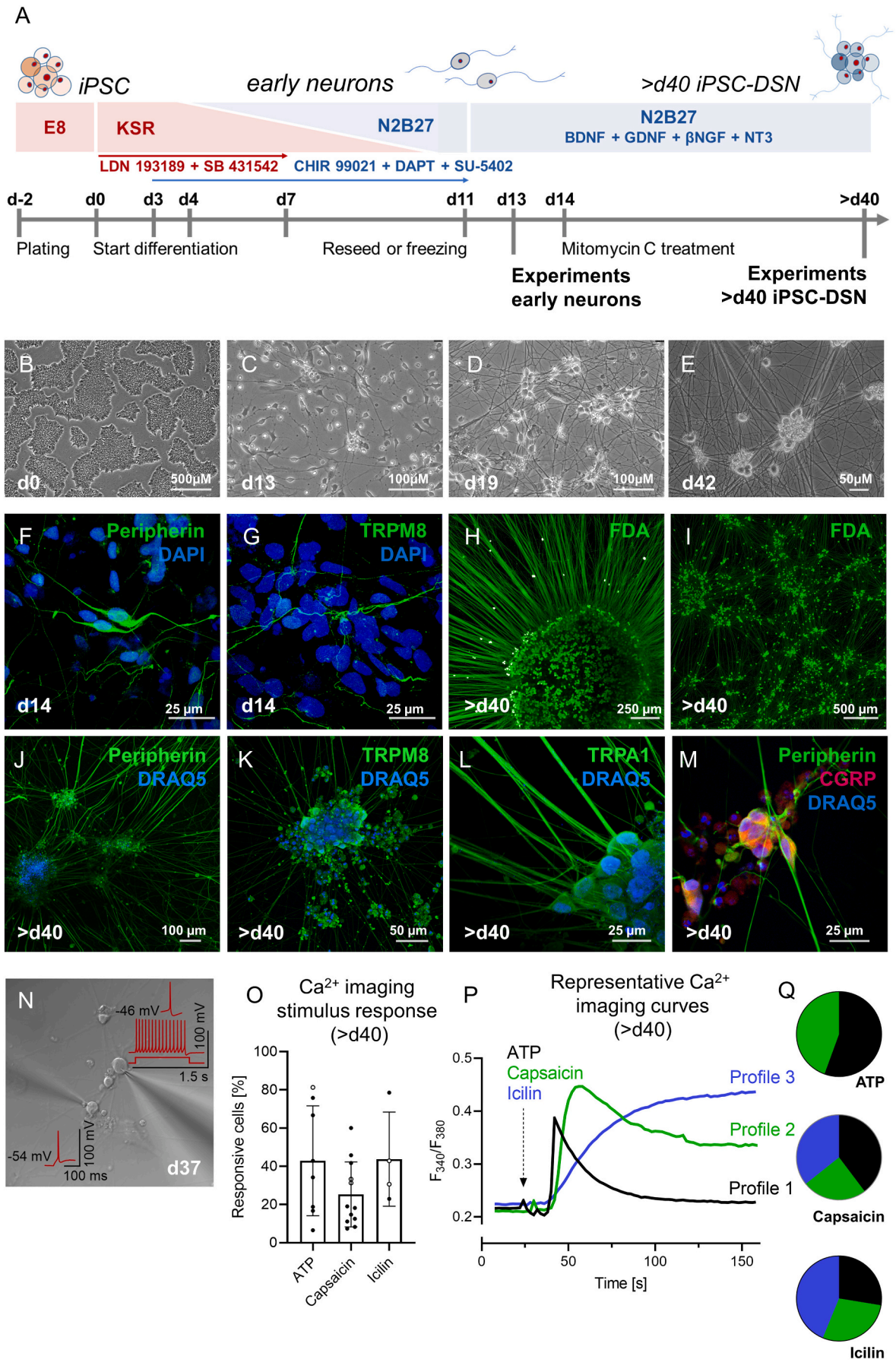

(caption on next page)

Fig. 1. Morphological and functional characterization of iPSC-DSN.
(A) Cells were cultured in E8 media until *differentiation* was commenced with dual SMAD inhibition (LDN19318, SB431542), followed by WNT activation (CHIR99021), Notch inhibition (DAPT) and inhibition of VEGF/FGF/PDGF (SU5402) for 11 days. Cells were cultured for at least 30 more days (maturation phase). (B-E) show representative phase contrast images of the *differentiation*, from stem cell colonies (B) to sensory neuron ganglia like structures (E). (F-G) show early neurons (d14) expressing peripherin (F) and TRPM8 (G). Ganglia-like structures (H) and extensively arborized neurons (I) were seen after maturation using live cell imaging with FDA, and J-M expressed typical markers of the peripheral nervous system (J, Peripherin; K, TRPM8; L, TRPA1; M, Peripherin and CGRP). Physiological resting state and action potentials were revealed in patch clamp experiments (N). >d40 iPSC-DSN were responsive to inflammatory stimuli (ATP, open circles 10 μM, filled circles 100 μM) and the TRPV1 agonist capsaicin (open circles 1 μM, filled circles 10 μM) and the TRPM8 agonist icilin (open circles 1 μM, filled circles 10 μM) in Ca^{2+} imaging experiments (O), and responded with a Transient Increase (Profile 1), Increase with Plateau (Profile 2) or Plateau (Profile 3, (P)), as quantitively shown in pie charts for the respective stimuli (Q).

contrast microscopy (Olympus BX-51WI) equipped with a digital camera (Olympus XM10). Recordings were performed using 4 Multiclamp 700B amplifiers (Molecular Devices) in current-clamp mode. Low-pass filtering was applied at 6 kHz using the amplifiers built in Bessel filter and digitized with a Digidata 1550 (Molecular Devices) at a sampling rate of 20 kHz. The pClamp 10.4 software package (Molecular Devices) was applied for data acquisition and analysis (Peng et al., 2017). *Intrinsic electrophysiological properties:* Series resistance was between 22 MΩ and 70 MΩ and measured in voltage-clamp mode using a 200 ms long 10 mV pulse. Resting state membrane potential (RMP) was determined as the mean of a 10 ms long baseline before the first step current injection after switching to current clamp mode. Action potentials (AP) were elicited by injecting a set of 1 s long current pulses starting at an amplitude of −100 pA increasing to 800 pA in increments of 50–300 pA. The first action potential elicited at rheobase was analyzed. A total of 11 cells were recorded. Up to 5 cells were recorded simultaneously.

2.4. Calcium live-cell imaging

Calcium imaging was performed as described previously (Von Der Ahe et al., 2018). iPSC-DSN were loaded with Fura-2 AM 5 μM (Life Technologies GmbH, Darmstadt, Germany) and 0.02% pluronic F-127 (Life Technologies GmbH, Darmstadt, Deutschland) for 30 min at 37 °C in a standard HEPES buffered solution prepared as 130 mM NaCl, 4.7 mM KCl, 1 mM $MgSO_4$, 1.2 mM KH_2PO_4, 1.3 mM $CaCl_2$, 20 mM Hepes and 5 mM glucose, pH 7.4. After incubation, cell cultures were washed with standard HEPES buffered solution, and 8-Chamberslides or 24-well plates were placed in an Olympus IX 81 microscope equipped with a Uplan FLN objective 40×/1.13 (Olympus Corporation, Tokyo, Japan).

Fluorescence signals were detected by a cooled CCD-camera at 1 Hz, and data processed using Xcellence imaging software (Olympus). Experiments were performed at room temperature. F340/380 ratios were calculated for all regions of interest (ROI) after background subtraction. Stock solutions were diluted in HEPES buffered solution and manually added in a 1:10 ratio to the wells to reach a final concentration of 1 or 10 μM capsaicin (HelloBio), 1 or 10 μM icilin (Tocris) and 10 or 100 μM ATP (Tocris). An F340/380 increase of >20% of baseline was considered as response. Calcium imaging was performed between maturation day 43 and 77 for both cell lines (Detailed description in Suppl. Mat. 1, Table 2).

2.5. Compound preparation

Paclitaxel (Adipogen), bortezomib (Cayman Chemical) and 5-fluorouracil (Sigma) were dissolved in DMSO, and cisplatin (Sigma) in sterile 0.9% NaCl to reach 6 mM stock solutions. Vincristine (Cayman Chemical), doxorubicin hydrochloride (Tocris) and lithium chloride (Sigma) were prepared as aqueous solutions with sterile water to reach a 1 mM or 600 mM (lithium chloride) stock solution. Final concentrations of 1 nM to 100 μM (cisplatin) or 100 pM to 10 μM (all other substances but lithium, which was used in 10 to 1000 μM concentrations) were applied for 24 h for cell viability and cytotoxicity experiments, unless otherwise stated. Concentrations of the vehicles were 1/600 DMSO (for experiments with paclitaxel, bortezomib and 5-fluorouracil), 1/100 NaCl 0.9% or water (for experiments with vinristine, doxorubicin) and 1/60 (NaCl 0.9%, experiments with cisplatin).

2.6. Comparative bright field imaging and automated microscopic imaging before and after 24 h of exposure to cytotoxic drugs

Comparative bright field images were taken with Cell3 iMager Duos (Screen Holdings Co., Ltd.), using automated image acquisition before and after 24 h of incubation with the cytostatic drugs (paclitaxel 10 μM, bortezomib 10 μM, vincristine 10 μM, cisplatin 100 μM, doxorubicin 10 μM, 5-fluorouracil 10 μM), or after 72 h following a 24 h incubation with concentrations close to the calculated IC_{50} (paclitaxel 1 μM, bortezomib 10 nM, vincristine 100 nM, cisplatin 10 μM). Opera Phenix High Content Screening System (Perkin Elmer, USA) was used for live cell imaging. Cells were incubated with fluoresceine diacetate (FDA, in DMSO, Invitrogen™, F1303) at 5 μg/ml for 5 min in N2B27. Media was completely removed after image acquisition, and cells were incubated with the cytostatic drugs for 24 h until cells were stained again with 5 μg/ml FDA. Images were taken automatically at pre-defined regions of interest and manually compared, and representative images selected.

2.7. Cell viability and cytotoxicity assays

Antineoplastic drugs were added to iPSC-DSN cultured in 96-well plates and incubated for 24 h if not otherwise stated. For cell viability and cytotoxicity, MTT and proteases assays (Promega CytoTox-Fluor Assay and CytoTox-Glo Assay) were applied according to the manufacturers' instructions and live/dead ratios of MTT/proteases assays were calculated and normalized to vehicle, as described previously (Von Der Ahe et al., 2018). The z-factor was calculated applying digitonin (200 μg/ml, sigma) for 24 h on iPSC-DSN d13, resulting in a mean value of 0.76 ± 0.13, indicating a large separation band (Zhang et al., 1999) (5 experiments pooled, see Suppl. Mat. 1, Table 3). Experiments to evaluate lithium chloride as potential neuroprotectant were performed with the same setup, but in a 72 h treatment challenge.

2.8. Transcriptome sequencing analyses

iPSC-DSN were maintained in geltrex coated 6-well plates at 10^6 cells/well as described above. After maturation until d44 - d49, three wells were either treated with DMSO at 1/6000 or paclitaxel at 1 μM for 24 h, and RNA was harvested with the Aurum™ Total RNA Mini Kit according to manufacturers' instructions, with a total RNA amount between 1.49 and 2.97 μg. RNA sequencing was performed by Brooks Life Sciences Genewiz® with PolyA selection for RNA removal, 2 × 150 bp sequencing configuration and 20–30 million reads per sample. 5 samples were analyzed ($n = 3$ DMSO treated vs. 2 paclitaxel treated).

Computational Methods. RNA Seq reads were mapped to human genome (GRCh38.p7) with STAR-version 2.7.3a (Dobin et al., 2013) using the default parameters. We obtained on average 80.2% uniquely mapped reads per sample. Reads were assigned to genes with featureCounts (Liao et al., 2014) with the following parameters: -t exon -g gene_id, gene annotation - Gencode GRCh38/v25. The differential expression analysis was carried out with DESeq2-version 1.22.1 (Love et al., 2014) using the default parameters. We kept genes that have at least 5 reads in at least 2 samples. Gene set enrichment analysis was

Table 1
Characterization of cytotoxic drugs. Cancer indication, mechanism of action and prevalence of neuropathy are reviewed by (Boehmerle et al., 2014). Elimination half-lifes, maximum and steady state concentrations vary according to indication, application scheme and individual metabolism. Due to small effect sizes for paclitaxel after 24 h of treatment, 72 h treatment was evaluated and compared to 5-fluorouracil as non-neurotoxic drug. Sources: paclitaxel (Rowinsky and Donehower, 1995; Hertz et al., 2018; Vermorken et al., 1984; Walle et al., 1995), bortezomib (Moreau et al., 2011; Reece et al., 2011; Schwartz and Davidson, 2004), vincristine (Yan et al., 2012; Yang et al., 2018; Van Den Berg et al., 1982; Nelson, 1982), cisplatin (Rajkumar et al., 2016; De Jongh et al., 2004; Urien and Lokiec, 2004), doxorubicin (Barpe et al., 2010; Bressolle et al., 1992), 5-fluorouracil (protracted venous infusion) (Yamada et al., 2003; Jodrell et al., 2001; Diasio and Harris, 1989).

Cytotoxic drug	Cancer indication (selection)	Mechanism of action	Prevalence of peripheral neuropathy [%]	Elimination half life	Maximum plasma concentration	Steady state concentration	>d40 iPSC-DSN Calculated IC_{50} [95% CI] for 24 h treatment, unless otherwise stated	d13 iPSC-DSN Calculated IC_{50} [95% CI]
Paclitaxel	Solid tumors including breast-, ovarian-, cervical-, non small cell lung cancer	Stabilization of the microtubule cytoskeleton	57–82%	~6 h	~2.7–7 μM	~0.2–0.5 μM	290 [12–5933] nM 72 h: 99.1 [27–479] nM	6.9 [2.2–19.5] nM
Bortezomib	Multiple myeloma	Proteasome inhibitor	36–64%	>40 h	~50 nM (*s.c.*) vs. *570 nM (i.v.)*	~3.5–5 nM	3.8 [2.2–6.8] nM	3.8 [2.9–4.8] nM
Vincristine	Miscellaneous: Leukemia, lymphoma, solid tumors	Inhibition of microtubule polymerization	43–91%	~8–90 h	~100–200 nM	~5–10 nM	66.3 [39.4–111.4] nM	1.7 [1.2–2.4] nM
Cisplatin	Solid tumors, including lung, head and neck, ovarian cancer and sarcoma	Platinum-DNA crosslinks	53–68%	~70 h	~15–35 μM	~2–14 μM	11.7 [6.4–22.0] μM	4.5 [3.2–6.4] μM
Doxorubicin	Solid and hematological malignancies including breast cancer, leukemia, lymphoma, lung cancer	DNA intercalation	<0.1% Cardiotoxic.	~28 h	~1.1 μM	~35–105 nM	408.8 [n.a.] μM	466 [354–611] nM
5-Fluorouracil	Solid tumors, including colon-, esophageal-, stomach-, pancreatic-carcinoma	Thymidylate synthase inhibitor, Inhibition of DNA replication	<0.1%	~8–20 min	0.8 μM	~0.4–0.8 μM	n.a. 72 h: n.a.	not applicable.

carried out with R/tmod package (Zyla et al., 2019).

2.9. Statistical analyses

Data were analyzed using Prism v8 (Graphpad Software, San Diego, CA). Data were checked for Gaussian distribution using Shapiro-Wilk normality test and histograms. Normally distributed data were analyzed with two-sided *t*-tests (2 groups). Data with low sample sizes or data not fulfilling the criterion of normal distribution were analyzed with Mann-Whitney-*U* test (2 groups). Cell viabilities were compared with one-way ANOVA and corrected for multiple comparison using Holm-Sidak's multiple comparison test (normally distributed data) or the Kruskal-Wallis test and corrected using the Dunn's multiple comparison test (data which were not normally distributed). Dose-response curves were calculated with non-linear regression models using GraphPad Prism (Log inhibitor vs. response, three parameters). All experiments with >d40 iPSC-DSN were replicated at least 3 times from at least 2 independently differentiated iPSC-DSN cultures (biological replicates) with 4 technical replicates for each condition (see detailed description in Suppl. Material 1, Table 1 and Suppl. Figs. 5–19). Data points with more than two standard deviations from the sample mean were treated as outliers and excluded from analysis, which was the case in 1.66% of the analyzed wells (See Suppl. Mat. 1, Table 1). Normally distributed data are presented as mean ± SD. Not normally distributed data are shown as median with interquartile ranges. Results for all 81 analyzed assays are shown in Suppl. Mat. 1, Figs. 5–19.

2.10. Data availability

Open data publishing guidelines were followed. Data are available in the *Data-in-Brief-Co-Submission*. RNA sequencing data discussed in this publication have been deposited in NCBI's Gene Expression Omnibus (Edgar, 2002) and are accessible through GEO Series accession number GSE173610 (https://www.ncbi.nlm.nih.gov/geo/query/acc.cgi?acc=GSE173610).

3. Results

3.1. Morphological and functional properties of iPSC-DSN

Sensory neurons were differentiated from iPSCs generated from two different, healthy donors according to the protocol published by Schwartzentruber et al. (2018). Briefly, iPSC-DSN underwent 11 days of *differentiation* to derive *early neurons* followed by a minimum of 30 days of *maturation* to derive *iPSC-DSN with typical functional properties of sensory neurons* (Fig. 1 A), as described below. Differentiation was started when 70–90% confluency was achieved (Fig. 1 B) and, soon after replating, we observed pseudounipolar neuronal cells (Fig. 1 C). After mitomycin c treatment, the few proliferating cells were eliminated and neurons formed ganglia-like structures (Fig. 1 D). After 40 days, morphologically pure neuronal cultures were observed (Fig. 1 E).

Early iPSC-derived neurons could be identified on day 14 by staining for peripheral sensory nervous system markers such as peripherin (Fig. 1 F). At that time some cells already expressed transient receptor potential cation channel subfamily M member 8 (TRPM8) which plays a role for temperature (cold) sensation (Fig. 1 G). By day 40, we observed large ganglia with extensive axons (Fig. 1 H + I). Subsets of neurons expressed peripherin, calcitonine gene related peptide (CGRP), transient receptor potential cation channel, subfamily A member 1 (TRPA1) and TRPM8 (Fig. 1 J-M) as well as the transient receptor potential cation channel subfamily V member 4 (TRPV4) (Suppl. Fig. 1 F). The channels are separately shown in Suppl. Fig. 1 A-G.

We examined electrophysiological properties of the neurons through whole cell patch-clamp recordings on day 33–37 (Fig. 1 N). We recorded 11 neurons which exhibited physiological resting membrane potentials of −51.5 ± 4.8 mV and input resistance of 395 ± 147 MΩ. They were

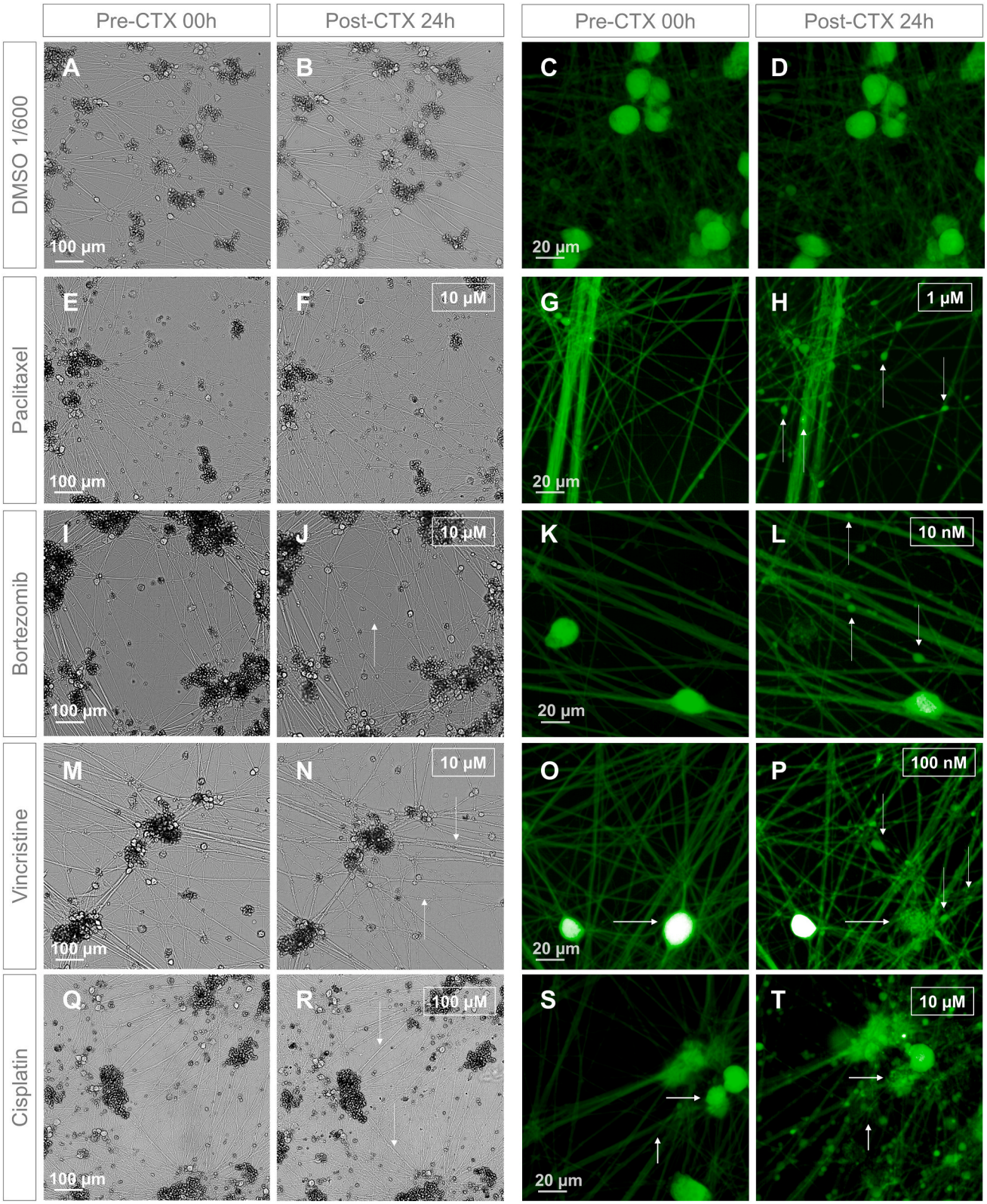

Fig. 2. Morphological changes of iPSC-DSN upon 24 h-treatment with neurotoxic drugs.
iPSC-DSN incubated for 24 h with a DMSO control did not show signs of neurodegeneration (A-D). Axonal blebbing as a sign of axonal damage was observed for all the 4 cytotoxic drugs after 24 h of incubation, modestly for paclitaxel (*E*-H), moderately for bortezomib (I-L) and most apparent for vincristine (M-P) and cisplatin (Q-T). At low concentrations of cytotoxic drugs near the calculated IC_{50}, signs of axonal damage were more sensitively seen using fluoresceine diacetate (FDA) dyed neurons and live cell imaging (right panels) than bright field images (left panels). Vertical white arrows indicate axonal blebbing, horizontal arrows highlight lost cells after 24 h incubation with cytotoxic drugs.

able to elicit action potentials upon step current injection exhibiting kinetics within the range of previous studies (amplitude = 88 ± 14 mV, half-width = 2.1 ± 1.1 ms, maximum rise slope = 123 ± 55 mV/ms) (Meents et al., 2019) (Suppl. Fig. 2 A-E).

Calcium imaging experiments showed that 43 ± 29% (SD) of >d40 iPSC-DSN (d43-d77) responded to adenosine trisphosphate (ATP) stimulation, an agonist of P2X/P2Y purinoreceptors which plays an important role for inflammatory pain. 25 ± 17% of the cells responded to capsaicin, an agonist of the TRPV1 receptor which plays an important role in nociception. Furthermore, 44 ± 25% of the cells responded to stimulation with icilin, a TRPM8 receptor agonist which implies that the receptors detected by immunofluorescence are indeed functional (Fig. 1 O). The number of responding cells was comparable between different doses of ATP/capsaicin/icilin which suggests that already the lower dose elicited a response saturation (Fig. 1 O). In general, we observed three different response patterns: a *transient response* (profile 1), a *transient response with subsequent plateau* (profile 2) and a *slow increase* (profile 3) (Fig. 1 P). When we analyzed the response profiles for each stimulus, we found that most iPSC-DSN responded to ATP with a transient Ca^{2+}increase or an increase with plateau (profile 1: 56 ± 33%, profile 2: 44 ± 33%). For capsaicin and icilin, all three response profiles were observed (capsaicin: profile 1: 41 ± 44%, profile 2: 25 ± 31%, profile 3: 36 ± 40%; icilin: profile 1: 28 ± 24%, profile 2: 29 ± 8%, profile 3: 44 ± 29%, Fig. 1 Q). In contrast, early iPSC-DSN (d14) showed low responses to very high concentrations of ATP but not to the other stimuli (1 mM ATP, Suppl. Fig. 2 F). Sequential stimulation of iPSC-DSN revealed a functional heterogeneity of cells within the cultures, with some iPSC-DSN sensitive to low concentrations of capsaicin (1 μM) and others only to higher concentrations (10 μM). Some cells reacted to icilin only but not to capsaicin (Suppl. Fig. 2 G), or to capsaicin and pH 6 or to either of the both stimuli (Suppl. Fig. 2 H), indicating differential sensitivity and specificity of different cells upon stimuli within the cultures as observed in dorsal root ganglia (DRGs) derived from humans (Schoepf et al., 2020; Li et al., 2015). Responsiveness in Ca^{2+} imaging experiments was shown for the cell lines BIHi005-A and BIHi004-B, and for directly differentiated neurons and neurons matured after thawing (detailed list of experiments in Suppl. Mat. 1, Table 2). In conclusion, >d40 iPSC-DSN show morphological features typical for primary dorsal root ganglia neurons, electrical activity of neurons and express functional receptors for environmental stimuli as would be expected in sensory neurons.

3.2. Sensitivity of iPSC-DSN to different clinically relevant cytotoxic drugs in a 24 h treatment regimen

In a next step, we were interested in how >d40 and early (d13) iPSC-DSN react to four clinically relevant drugs used for chemotherapy with a known neurotoxic side effect profile in comparison to two compounds which do not usually cause CIPN in humans. Pharmacological and clinical characteristics of substances used in this study are summarized in Table 1. 24 h-incubation with 1:600 DMSO (vehicle) did not lead to morphological changes of iPSC-DSN cell bodies or axons (Fig. 2 A-D). After 24-h exposure with 10 μM paclitaxel, no morphological changes were detected in bright field imaging (Fig. 2 E + F). Using live cell imaging with FDA, we observed axonal blebbing in some areas of the culture but not all, while cell bodies were mostly unaffected (Fig. 2 G +

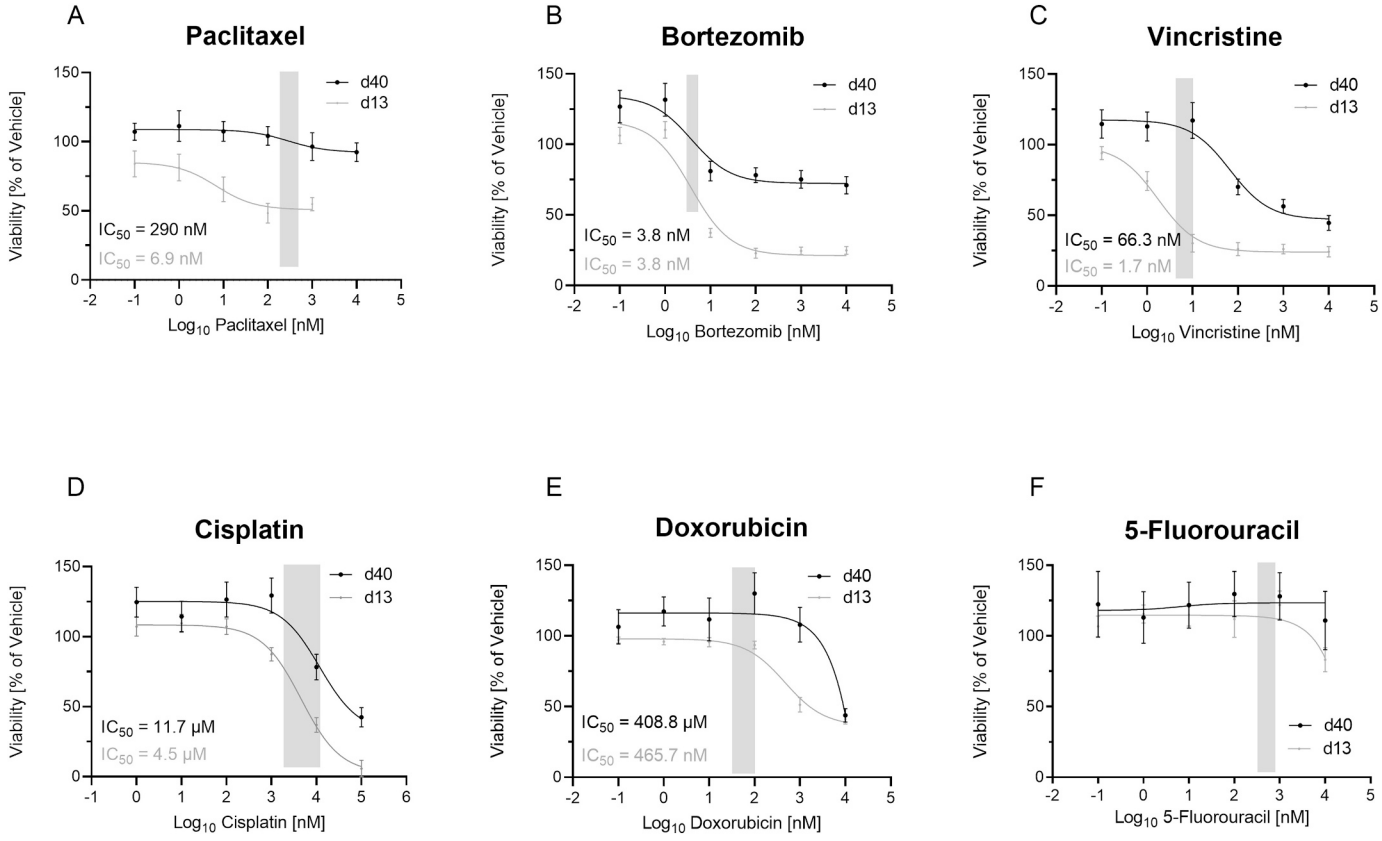

Fig. 3. Effect of cytotoxic drugs on cell viability (24 h treatment).
Curves show the calculated live/dead ratio from MTT and protease assays as mean viability with 95% confidence interval. (A-D) show dose-response curves of the tested neurotoxic drugs, and (E-F) demonstrate results from the incubation with the non-neurotoxic drugs doxorubicin and 5-fluorouracil, revealing high substance specificity. <d40 iPSC-DSN (black line) show IC_{50} close to the steady concentrations used in patients (grey shading), with early neurons (grey line) being more sensitive. Number of pooled experiments (>d40 neurons/d13 neurons): paclitaxel 7/3, bortezomib 9/4, vincristine 11/6, cisplatin 9/5, doxorubicin 3/3, 5-fluorouracil: 4/3. All assays with the respective cell lines that were used are shown separately in Suppl. Fig. 5–18.

H). 24-h exposure to bortezomib induced axonal blebbing and fragmentation of the plasma membranes (Fig. 2 I-L). The most obvious morphological changes were observed for vincristine and cisplatin, showing the disappearance of cells, axonal blebbing and membrane fragmentation for vincristine (Fig. 2 M-P) and cisplatin (Fig. 2 Q-T). These changes were not present after the treatment with the non-neurotoxic drugs doxorubicin (Suppl. Fig. 3 A + B) and 5-fluorouracil (Suppl. Fig. 3 C + D). Morphological indicators of cell body and axonal damage were also observed in bright field microscopy if *low* concentrations of chemotherapy near the calculated IC_{50} were applied for 24 h, then removed, and imaged 48 h after removal. In contrast, no substantial changes were observed for vehicle (Suppl. Fig. 4 A-J). Effects were again smaller for paclitaxel (Suppl. Fig. 4 C—D) and bortezomib (Suppl. Fig. 4 *E*-F) but remarkable for vincristine and cisplatin (Suppl. Fig. 4 G-J).

We evaluated the dose-dependent effects of chemotherapy with paclitaxel (PTX), bortezomib (BTZ), vincristine (VIN) and cisplatin (CIS) in >d40 and early iPSC-DSN. 24 h exposure of iPSC-DSN with PTX, BTZ, VIN and CIS led to a dose-dependent decline in cell viability with calculated IC_{50} in or close to the steady state concentration applied in a clinical setting in patients. In >d40 iPSC-DSN, paclitaxel showed the smallest effect sizes with a correspondingly high variability of the IC_{50} as not in all experiments stable plateaus were reached for the lowest and highest PTX concentrations (IC_{50} 290 nm [95% CI 12–5933]). Early iPSC-DSN were more sensitive to PTX with an IC_{50} of 6.9 nM [95% CI 2.2–19.5] which is two orders of magnitude lower than the clinically applied steady state concentration of about 0.5 μM in humans (Table 1, Fig. 3 A). For bortezomib, >d40 iPSC-DSN and early neurons showed an equal IC_{50} of 3.8 nM [95% CI 2.2–6.8 and 2.9–4.8] which is close to the clinically applied steady state concentration of 3.5–5 nM in humans (Table 1). The viability in concentrations between 10 nM and 10 μM was much lower in early iPSC-DSN indicative for a higher vulnerability of early iPSC-DSN to bortezomib (Table 1, Fig. 3 B). For vincristine and cisplatin, IC_{50} were higher in >d40 iPSC-DSN (vincristine: IC_{50} 66.3 nM [95% CI 39.4–111.4]; cisplatin: 11.7 μM [95% CI 6.4–22.0]) than in early iPSC-DSN (vincristine: IC_{50} 1.7 nM [95% CI 1.2–2.4]; cisplatin: 4.5 μM [95% CI 3.2–6.4]) and close to the clinically applied steady state concentrations in humans of about 5–10 nM for vincristine and 2–14 μM for cisplatin (Table 1, Fig. 3 C—D. All 81 assays are shown separately and pooled in Suppl. Figs. 5–19).

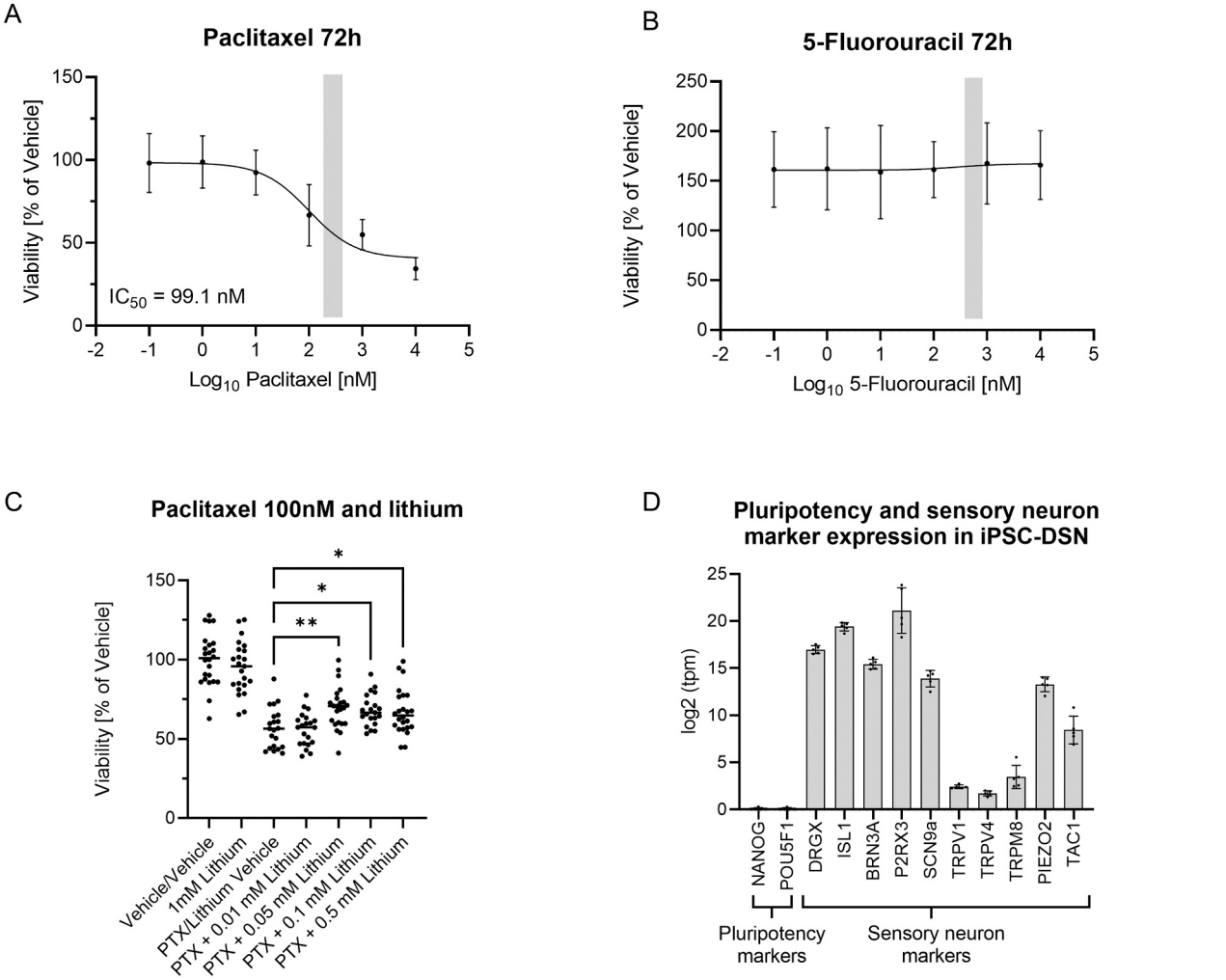

Fig. 4. Effects of prolonged incubation with paclitaxel or 5-fluorouracil, evaluation of lithium as potential neuroprotectant and transcriptome analyses of iPSC-DSN. (A) Shows the calculated live/dead ratio as mean viability with 95% confidence interval from MTT and proteases assays of iPSC-DSN incubated with paclitaxel for 72 h or (B) 5-fluorouracil for 72 h. A decline in cell viability in clinically relevant ranges (grey shading) was detected for paclitaxel, but not for 5-FU. (C) Shows moderate neuroprotective effects of iPSC-DSN treated with paclitaxel at 100 nM for 72 h when cells were co-incubated with lithium at 0.05–0.5 mM. Curves show dot plots calculated from live/dead ratio of MTT and proteases assays. (D) Shows the expression of typical markers of the sensory nervous system in our iPSC-DSN sample (>d40) as revealed by global transcriptome analyses, while typical markers of stem cells were not expressed. Number of pooled experiments (>d40 neurons): paclitaxel $n = 5$, 5-fluorouracil $n = 3$, paclitaxel 100 nM and lithium $n = 5$. All assays pooled in Fig. 4 (A-C) are shown separately in Suppl. Fig. 5–19. Transcriptome data with tpm are given in Suppl. Mat. 2.

3.3. Substance specificity of iPSC-DSN

As opposed to PTX, BTZ, VIN and CIS, the exposure of >d40 iPSC-DSN with the clinically non-neurotoxic chemotherapy substances doxorubicin and 5-fluorouracil only led to a decrease in cell viability in much higher than clinically relevant dosages with an IC_{50} of 409 μM for doxorubicin which is ~5000-fold higher than the usually observed steady state concentrations in humans (Table 1, Fig. 3 *E*-F). *Early* iPSC-DSN showed a relevant decline in cell viability with an IC_{50} for doxorubicin of 466 nM. For 5-fluorouracil, no IC_{50} could be calculated for >d40 iPSC-DSN nor early iPSC-DSN as no plateau was reached for the highest concentrations applied (10 μM), a concentration which is more than 10-fold higher than the clinically relevant steady state concentration (Table 1, Fig. 3 E-F). In conclusion, the treatment of >d40 iPSC-DSN with neurotoxic chemotherapy in clinically relevant dosages induced neurodegeneration with a dose-dependent decline in cell viability which was not the case for non-neurotoxic chemotherapy drugs.

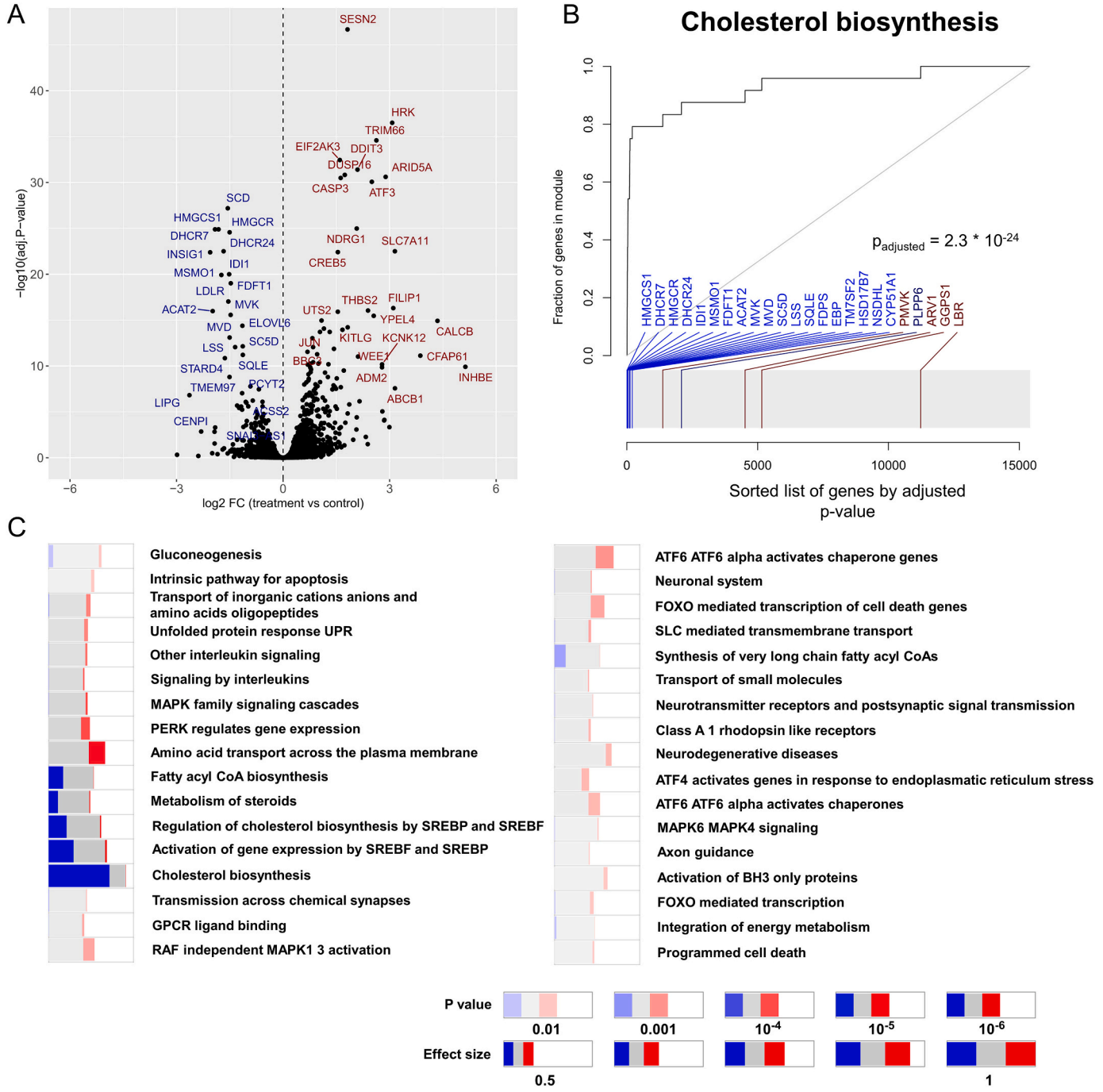

Fig. 5. Transcriptome sequencing analyses of iPSC-DSN treated with 1 μM paclitaxel for 24 h.
(A) Differential gene expression upon paclitaxel treatment. X-axis shows gene log2 fold changes, Y-axis is -log10 (adj.*P*-value). (B) Evidence plots for significantly deregulated gene sets. X-axis is the list of genes sorted by the adjusted *p*-value, Y-axis is the fraction of genes in this particular gene set. Bright colors show genes with adj. P-value <0.05. Red are up- and blue are down-regulated genes (more differentially-regulated genes and gene sets are given in Suppl. Mat. 2 and 3). (C) Panel plots show the top deregulated pathways from MsigDB Reactome gene set collection. The effect size represents the area under the curve (from Fig. 5 B). The brightness of the boxes shows the significance.

3.4. 72 h treatment of >d40 iPSC-DSN with paclitaxel but not with 5-fluorouracil leads to a decreased cell viability

As only small effects on cell viability were observed for paclitaxel upon 24 h treatment (100pM: 108.8 [95% CI 104.2–113.8]; 10 μM: 92.2 [95% CI 79.4–99.6]), we were interested if prolongation of the incubation time increases neurotoxic effects of paclitaxel on iPSC-DSN. A prolonged incubation period is justified from a clinical standpoint, as paclitaxel-induced neurotoxicity in the peripheral nervous system usually develops only after more than 50% of scheduled cycles. As a control for substance specificity we chose the non-neurotoxic drug 5-fluorouracil. We observed a dose-dependent decline of cell viability of >d40 iPSC-DSN following 72 h paclitaxel treatment but not for 5-fluorouracil treatment (PTX: IC_{50} 99.1 [95% CI 26.7–479.1] nM, cell viability 100pM: 98.4% [95% CI 89.6–107.4%], 10 μM: 40.6% [95% CI 27.5–51.6%]; 5-FU: IC_{50} 287.7 nM [95% CI n.a.], see Fig. 4 A-B). This

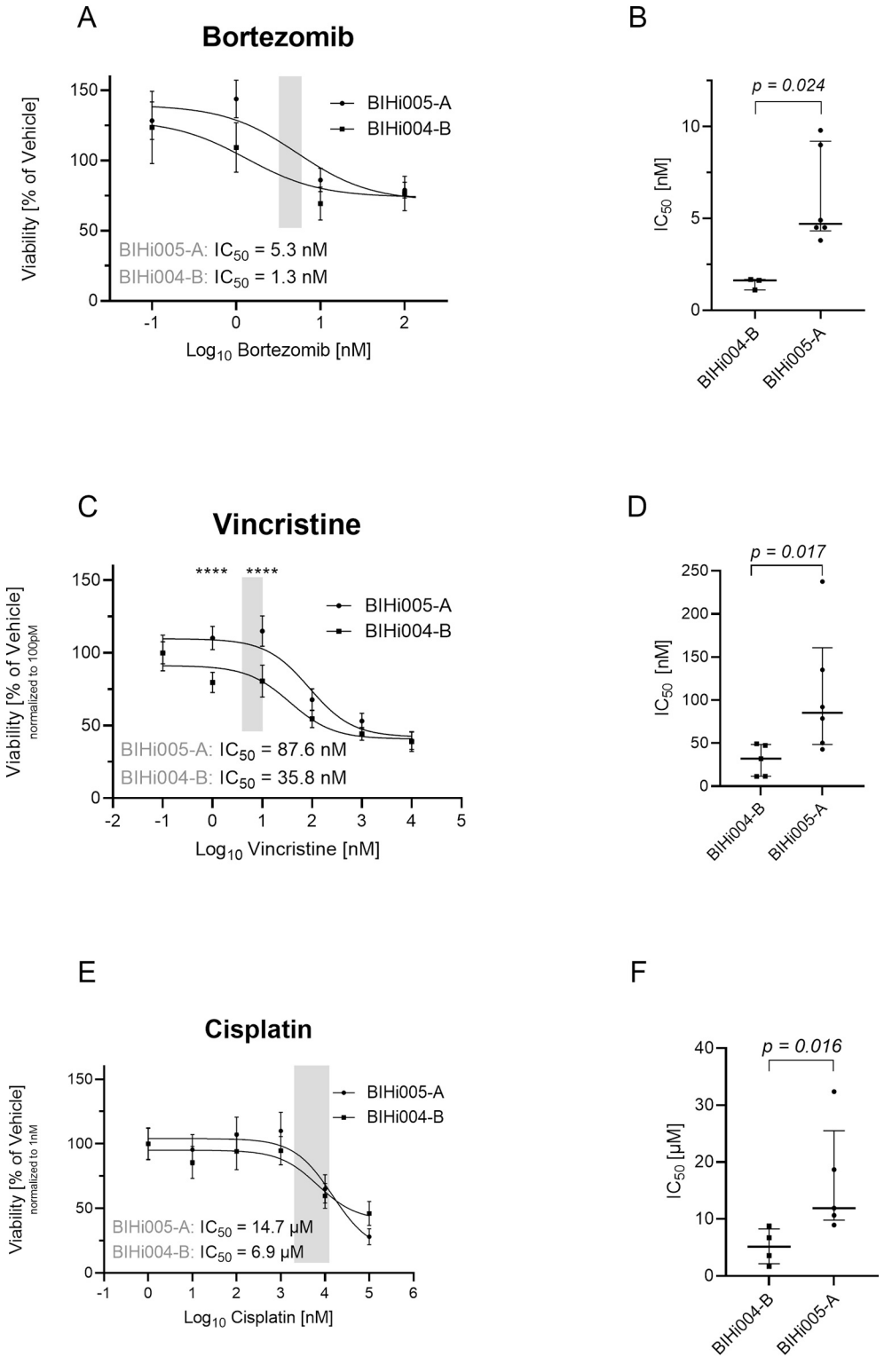

Fig. 6. Findings in iPSC-DSN cell lines derived from two different healthy donors. Curves show mean viability with 95% confidence interval. IC_{50} in the scatter plots were calculated for each experiment separately and given as median with interquartile range. The cell line BIHi004-B showed lower viabilities after 24 h incubation with bortezomib (A), correspondingly, with a significantly lower IC_{50} (B), which also held true for vincristine (C—D). Viabilities for cisplatin were similar between the cell lines (E), but again with lower calculated IC_{50} for BIHi004-B. Number of pooled experiments (cell line BIHi005-A/BIHi004-B): bortezomib 6/3, vincristine 6/5, cisplatin 5/4. All assays are shown separately in Suppl. Fig. 5–18.

indicates preserved substance specificity for neurotoxic effects in >d40 iPSC-DSN after prolonged treatment for 72 h.

3.5. Evaluation of lithium as potential neuroprotectant in the iPSC-DSN model

We next investigated lithium which was established in animal models as a neuroprotective compound for paclitaxel-induced neurotoxicity (Mo et al., 2012; Sanchez et al., 2020). We found that cytotoxic effects of a 72 h exposure to 100 nM paclitaxel can be partly prevented by co-incubation with clinically relevant concentrations of lithium chloride (50, 100, 500 μM). 100 nM paclitaxel exposure lead to a decline in cell viability of iPSC-DSN to 56.7% after 72 h (95% CI 50.9–62.5%) whereas the administration of 1 mM lithium-chloride did not affect cell viability as compared to vehicle (Vehicle: 100%, 95% CI 93.0–107.0; 1 mM lithium-chloride: 95.0%, 95% CI 87.9–102.0, ANOVA $p = 0.37$). Co-incubation with 50, 100 and 500 μM of lithium-chloride attenuated the cytotoxic effects of 100 nM PTX as compared to co-incubation with lithium-vehicle (50 μM: 69.8% [95% CI 64.1–75.6%, ANOVA, $p = 0.0079$], 100 μM: 68.0% [95% CI 63.5–72.6%, ANOVA, $p = 0.029$], 500 μM: 67.2% [95% CI 61.1–73.2%, ANOVA, $p = 0.031$], see Fig. 4 C). This indicates moderate neuroprotective effects of lithium-chloride in concentrations between 50 μM and 500 μM.

3.6. Transcriptome sequencing analyses of iPSC-DSN treated with 1 μM paclitaxel for 24 h

As effects on cell viability and axonal morphology were small after 24 h of treatment with paclitaxel but remarkable after 72 h of treatment, we were interested how paclitaxel in a dosage above the IC_{50} affects the transcriptome of iPSC-DSN *before* cell death occurs, and if the model is capable of replicating genes and gene subsets known from animal experiments. All 5 analyzed samples of iPSC-DSN (DMSO treated $n = 3$, paclitaxel 1 μM $n = 2$) expressed typical markers of iPSC-DSN according to Schwartzentruber et al. (2018) such as dorsal root ganglia homeobox (DRGX), Nav 1.8 (SCN9a) or Piezo-type mechanosensitive ion channel component 2 (Piezo2), whereas, expectedly, typical pluripotency markers such as NANOG or Oct-4 (POU5F1) were not expressed (Fig. 4 D; transcripts per kilobase million [TPM] for all analyzed genes are given in Suppl. Mat. 2).

RNA-Sequencing analyses revealed 319 significantly differentially ($p_{adjusted} < 0.01$) expressed genes out of which 227 were upregulated and 92 downregulated (Suppl. Material 3). 84 of the upregulated and 33 of the downregulated changed expression by at least 2 fold (see volcano plot, Fig. 5, A).

Upregulated genes involve known neuronal injury markers such as the *Activation Transcription Factor* (ATF3), stress-inducible proteins such as *Sestrin-2* (SESN2), apoptosis associated genes such as *Caspase 3* (CASP3), the JUN proto-oncogene (JUN) or BCL2-interacting proteins such as BBC3 or Harakiri (HRK). Also, vasoactive substances and pain inducing neuropeptides of the calcitonine gene related peptide family such as CALCB and adrenomedullin (ADM) were found amongst the top 50 differentially regulated genes. Other upregulated pain associated genes involve the Phosphoinositide Interacting Regulator Of Transient Receptor Potential Channels (PIRT) (Kim et al., 2008), and inflammation associated genes such as tumor necrosis factor alpha receptors (TNFRSF9, TNFRSF10B) or the Matrix Metalloproteinase 10 (MMP10). Four out of the top 50 differentially-expressed genes encode either mitochondrial enzymes (Mitochondrial Phosphoenolpyruvate Carboxykinase 2, PCK2; Acyl-CoA Synthetase Short Chain Family Member 2, ACSS2) or proteins that influence mitochondrial function (BCL2 Binding Component 3, BBC3; Eukaryotic Translation Initiation Factor 2 Alpha Kinase 3, EIF2AK3) (Suppl. Mat. 3).

Downregulated genes involve pathways of sterol homeostasis, glucose homeostasis and lipogenesis, e.g., 3-Hydroxy-3-Methylglutaryl-CoA Synthase 1 (HMGCS1), Insulin Induced Gene 1 (INSIG1) or ELOVL Fatty Acid Elongase 6 (ELOVL6) (Fig. 5 A; Suppl. Fig. 20). Gene set enrichment analysis outlined significant deregulation of genes involved in cholesterol biosynthesis pathways, PERK regulated genes and genes involved in amino acid transport across the membrane (Fig. 5 B-C; Suppl. Mat. 3). In summary, there is a significant overlap of the above-mentioned genes and gene sets outlined by unbiased global differential transcriptome analyses with pathways known from the literature of neuropathy, pain and neurodegeneration (discussed in more detail below).

3.7. Susceptibility of iPSC-DSN derived from two different healthy donors to neurotoxic chemotherapy

In a next step, we assessed sensitivity to cytotoxic drugs in iPSC-DSN derived from genetically different donors (cell lines BIHi004-B and BIHi005-A). Interestingly, we observed preliminary evidence for a differential susceptibility of >d40 iPSC-DSN derived from these cell lines to neurotoxic chemotherapy with bortezomib, vincristine and cisplatin as measured by different IC_{50} and partly different viabilities in concentrations close to the IC_{50}. In the case of bortezomib, IC_{50} concentrations were significantly lower in iPSC-DSN derived from donor BIHi004-B compared to donor BIHi005-A (median IC_{50} = 1.62 nM [95% CI 1.1–1.67] vs. 4.70 nM [95% CI 3.80–9.80], Mann-Whitney-U, $p = 0.024$; Fig. 6 A + B). Cell viabilities pointed into the same direction and were numerically, but not significantly, lower in cells derived from donor BIHi004-B than BIHi005-A when incubated with 1 nM (median viability = 101.2 nM [95% CI 89.2–127.7 vs. 137.0 nM [95% CI 123.0–151.7], Kruskal-Wallis test $p = 0.22$). There were no remarkable differences in very high or very low concentration ranges (Fig. 6 A + B). For vincristine, we observed a lower IC_{50} in cells derived from donor cell line BIHi004-B compared to BIHi005-A (median IC_{50} = 31.9 nM [95% CI 11.3–49.2] vs. 85.3 nM [95% CI 42.8–237.6], Mann-Whitney-U, $p = 0.017$, Fig. 6 C + D), and lower cell viabilities in cells from the donor BIHi004-B than BIHi005-A at 1 nM (median 85.0 nM [95% CI 72.8–86.7] vs. 107.3 nM [95% CI 102.2–118.1], ANOVA, $p < 0.0001$) and 10 nM (median 75.8 nM [95% CI 69.6–91.6] vs. 112.3 nM [95% CI 104.6–125.4], ANOVA, $p < 0.0001$). There were no differences in cell viabilities for very low (100pM) or high (100 nM – 10 μM) vincristine concentrations (Fig. 6 C + D). Exposure to cisplatin likewise affected iPSC-DSN derived from donor BIHi004-B more than iPSC-DSN from donor BIHi005-A, with an IC_{50} which was again lower in cell line BIHi004-B than in BIHi005-A (median IC_{50} = 5.1 μM [95% CI 1.7–8.8] vs. 11.9 μM [95% CI 9.0–32.4], $p = 0.016$, Fig. 6 E + F). Taken together, these results suggest a higher susceptibility to neurotoxic chemotherapy of iPSC-DSN derived from the donor BIHi004-B than BIHi005-A in dosage ranges which are in or close to the clinically applied concentrations. This, however, has to be interpreted cautiously as we do not have any clinical data of the donors, and as they differ in sex and ethnicity.

4. Discussion

In summary, this study models biological effects of chemotherapy induced neurotoxicity in human iPSC-derived sensory neurons: We observed a dose dependent decline in cell viability *in* or *close* to clinically measured steady state concentrations of the neurotoxic drugs paclitaxel, bortezomib, vincristine and cisplatin after 24 h of treatment. This effect is substance specific, as no relevant decline was observed for doxorubicin and 5-fluorouracil, cytotoxic drugs which do not typically induce CIPN. Correspondingly, morphological signs of neurodegeneration were observed for the neurotoxic drugs but not for the non-neurotoxic drugs or vehicle. Effects on cell viability and axonal integrity were small for paclitaxel after 24 h, but prominent if treatment was prolonged to 72 h. Substance specificity was preserved in the 72 h treatment regimen as 5-fluororuacil did not affect iPSC-DSN cell viability. We further investigated paclitaxel induced neurotoxicity with global transcriptome

analyses in the interval *before* apparent cell death occurs, which revealed the differential expression of genes involved in neuronal injury, cell death and metabolic pathways, replicating known genes and gene sets from animal based disease models. Co-administration of paclitaxel with lithium partly prevented neurotoxic effects, demonstrating the applicability of the human iPSC-DSN model to evaluate neuroprotective strategies. Cells differentiated from the donor BIHi004-B were more susceptible to neurotoxic compounds than cultures from the cell line BIHi005-A, which could be due to a donor-specific susceptibility of neurotoxic side effects as known from patients.

4.1. Morphological signs of axonal damage

The iPSC-DSN model was able to mimic the axonal damage induced by neurotoxic drugs. Axonal blebs are known to appear in still-viable cells when apoptosis is commenced and precede Wallerian degeneration (Sebbagh et al., 2001; Wang et al., 2012). Correspondingly, previous histological analyses of rodent sciatic and caudal nerves after cytotoxic treatment showed axonal loss for paclitaxel, bortezomib, vincristine and cisplatin and reduced sensory nerve action potentials, which correlates with the finding of sensory axonal neuropathy in humans (Boehmerle et al., 2015). A decreased neurite growth was shown in early iPSC-derived peripheral neurons and induced sensory neurons after administration of cytotoxic drugs (Wing et al., 2017; Vojnits et al., 2019). In our study, all four tested neurotoxic substances led to axonal blebbing after 24 h-incubation in iPSC-DSN. The effect was most pronounced for vincristine and cisplatin, moderate for bortezomib and small for paclitaxel. Detection of morphological changes was more sensitive when cells were live cell stained with FDA compared to bright field microscopy. Remarkably, these morphological signs were also observed in bright field imaging when concentrations of vincristine and cisplatin at low dosages were applied for 24 h and the and observation by microscopy done 48 h after removal of the treatment. This indicates that neurodegenerative pathways may already be activated within the first 24 h without being phenotypically apparent yet.

4.2. Effect of cytotoxic drugs on iPSC-DSN cell viability

We found iPSC-DSN to be sensitive to all four tested neurotoxic drugs in clinically relevant concentrations in a 24 h treatment regimen as measured by cell viability assays. For the two drugs that do not cause neuropathy in humans, doxorubicin and 5-fluorouracil, no decrease was observed in clinically relevant concentrations (5-fluorouracil) or noted only in concentrations higher than clinically relevant steady state concentrations or only in d13 iPSC-DSN (doxorubicin), indicating high substance specificity of >d40 iPSC-DSN. In the case of paclitaxel, we observed small effects on cell viability after 24 h similar to findings from another recent study (Xiong et al., 2021), which is why we tested a prolonged treatment of 72 h. From a clinical standpoint, this can be justified as paclitaxel-induced neurotoxicity in the peripheral nervous system usually develops only after more than 50% of scheduled cycles (Boehmerle et al., 2014). In the case of longer incubation with paclitaxel, we observed pronounced effects which allow comparative analyses or evaluation of neuroprotective strategies. Substance specificity was preserved even after 72 h treatment as no decrease of cell viability or neuronal morphology could be detected for the non-neurotoxic drug 5-fluorouracil. These findings suggest a 24 h treatment regimen is sufficient to study neurotoxic effects of bortezomib, vincristine and cisplatin while 72 h should be used for paclitaxel.

4.3. Transcriptome analyses of iPSC-DSN exposed to paclitaxel in the time interval before morphologically apparent cell death

Unbiased global transcriptome analyses of iPSC-DSN exposed to paclitaxel showed a remarkable overlap with previously reported candidate genes that are upregulated in animal-based peripheral nerve injury models, such as the activation transcription factor 3 (ATF3) (Omura et al., 2015; Seijffers et al., 2007; Pereira et al., 2019), Dual Specificity Phosphatase 4 (DUSP4) (Chandrasekhar et al., 2021), stress-inducible genes such as sestrin-2 (SESN2) or the DNA Damage Inducible Transcript 3 (DDIT3) (Kallenborn-Gerhardt et al., 2013; Syc-Mazurek et al., 2017). Interestingly, genes which belong to apoptotic pathways such as Casp3, HRK, JUN or BCL2 Binding Component 3 (BBC3) were already activated in this time window before cell death or severe axonal injury is completed, and were previously reported to be involved in the pathogenesis of peripheral neuropathies (Feinberg et al., 2017; Hantke et al., 2014).

The top-50 differentially expressed genes also involved the pain inducing nociceptive peptides calcitonine gene related peptide (CALCB) or adrenomedullin (ADM) which co-mediate migraine or paclitaxel induced neuropathic pain (Pittman et al., 2014; Li et al., 2018). In this context, we also found an upregulation of the gene encoding *PIRT [Phosphoinositide Interacting Regulator of TRP]*, a nociceptor membrane protein sensitizing TRPV1 channel activity (Kim et al., 2008) as well as inflammatory pathways, e.g., TNF alpha receptors and a matrix metalloproteinase which were reported to be involved in peripheral and central pain modulation (Spicarova et al., 2011) and CIPN (Gu et al., 2020). Interestingly, four of the top 50-differentially expressed genes encoded either mitochondrial enzymes (PCK2, ACSS2) or proteins involved in mitochondrial function (BBC3; EIF2AK3) (Stelzer et al., 2016). This is noteworthy as changes in mitochondrial bioenergetics were recently reported in paclitaxel-induced neuropathies (Xiong et al., 2021; Duggett et al., 2017) and preclinical neuritis models (Muke et al., 2020). It should be evaluated if these genes translate into protein and function, e.g., measuring pain associated-neuropeptides, changes of electrophysiological properties or sensory neuron bioenergetics in relation to the clinical phenotype once patient-specific iPSC-DSN are available.

Significantly downregulated genes were found to be enriched in cholesterol biosynthesis and fatty acid metabolism pathways which are necessary for axon regeneration (Goodrum et al., 2000), and knockdown of these candidates has been shown to be involved in the pathogenesis of peripheral neuropathy (Cermenati et al., 2015). Recently, downregulation of the same gene cluster of cholesterol synthesis enzymes (DHCR24, MSMO1, IDI1 and HMGCS1) was reported in an animal model of central neurodegeneration (Canet-Pons et al., 2021), and the upregulation pERK associated genes corroborates recent findings of paclitaxel-induced neuropathy in cultured rodent DRGs (Li et al., 2021).

Albeit differential transcriptome analyses in iPSC-DSN remarkably parallel some previously described genes and gene sets from animal experiments or chronic pain conditions (Li et al., 2021; Wangzhou et al., 2021), further experiments with patient-specific cell lines and different neurotoxic versus non-neurotoxic therapies are needed to separate unspecific epiphenomena of neuronal injury or cellular stress response from biologically meaningful mechanisms for the pathogenesis of neurodegeneration and pain.

4.4. iPSC-DSN as a platform to evaluate neuroprotective compounds

Previously, our research group and others demonstrated that lithium, a medication used to treat bipolar disorder, can attenuate paclitaxel-induced peripheral (Mo et al., 2012; Sanchez et al., 2020) and central (Huehnchen et al., 2017) neuronal damage in cell and animal-based models. We thus tested lithium ions as neuroprotectant in iPSC-DSN treated with paclitaxel (Sproule, 2002), and found moderate dose dependent neuroprotective effects of lithium in concentrations in clinically applied concentrations. These results encourage the use of iPSC-DSN as a preclinical animal-free platform for drug discovery.

4.5. Outlook - Cell line dependent toxicity as a marker to predict differential susceptibility to CIPN?

An important clinical characteristic of CIPN is that about 20–30% of patients receiving different chemotherapeutic regimes do not develop CIPN at all and the other 70–80% develop CIPN to varying degrees (Boehmerle et al., 2014; Seretny et al., 2014). In this study, we used iPSC from two different healthy donors of different sex and ethnicity who never underwent chemotherapy. It remains to be shown whether iPSC-derived sensory neurons would predict CIPN susceptibility to specific compounds for individual patients and potentially even help identify preventive treatments. The two cell lines we applied had different susceptibilities to neurotoxic chemotherapy. Dependent on regimen and observation period, the prevalence of CIPN increases up to 80% (Seretny et al., 2014), which highlights the necessity to establish tools to monitor, predict and prevent CIPN. While genome wide association studies outlined certain SNP loci as genetic risk factors (Mahmoudpour et al., 2018) and serum neurofilament light chain (sNFL) shows potential as biomarker of chemotherapy-induced neuroaxonal damage in rodents (Meregalli et al., 2020) and patients (Kim et al., 2020), the individual prediction of side effects is not yet possible for CIPN. Previously, donor-specific susceptibility to doxorubicin-induced cardiomyopathy could be recapitulated in iPSC-derived cardiomyocytes from patients with and without heart failure after chemotherapy (Burridge et al., 2016). These findings encourage the establishment of iPSC-derived neuronal models to study the underlying mechanisms of the individual susceptibility to neurotoxic effects. This will be possible when experimental results from cell lines of patients with and without CIPN are combined with the clinical phenotype.

Animal models for CIPN have been used for decades (Boehmerle et al., 2015; Cavaletti et al., 1992; Boehmerle et al., 2006; Röytta and Raine, 1985), despite some differences in their clinical presentation or electrophysiological properties (reviewed by Rostock et al. (2018), Eldridge et al. (2020)) and ethical issues. Recent studies foster the idea to apply *reduced* DRG-based in-vitro systems as they reproduce the same biological and physiologic responses known from whole animal models (Li et al., 2021), which also held true in iPSC-DSN. Stem-cell based neuronal models may complement these in-vitro approaches of pain and neurodegeneration research, along with essentially contributing to the 3R principle.

5. Conclusions

In summary, this study establishes the feasibility of human iPSC-DSN to model biological effects of chemotherapy induced neurotoxicity. Substance specific effects of neurotoxicity were observed upon treatment with clinically relevant concentrations of neurotoxic chemotherapy. Unbiased global transcriptome analyses confirmed the expression of relevant genes and gene sets known from animal models, and the previously demonstrated neuroprotective effects of lithium could be replicated in the human iPSC-DSN model. This underlines its potential utility investigating the pathomechanisms of CIPN and enables the development of novel neuroprotective strategies. Different sensitivities of iPSC-DSN derived from different healthy donors may hint towards individually determined CIPN vulnerability known from patients. The possibility to relate multi-omic data to functional readouts and clinical phenotype encourages patient-specific approaches to study the underlying mechanisms of CIPN in vitro. This could facilitate the discovery of individual predictive markers and the development of therapies to prevent or treat neurodegeneration and neuropathic pain.

Supplementary data to this article can be found online at https://doi.org/10.1016/j.nbd.2021.105391.

Declaration of Competing Interest

The authors report no conflict of interest.

Acknowledgements

We thank Petra Loge for excellent technical assistance, and Judit Küchler, Kristin Fischer, Claudia Schaar, Janine Cernoch and Tanja Fisch of the BIH Stem Cell Core Facility for their invaluable help in stem cell culture and maintenance. We thank Dr. Dorette Freyer for sharing her extensive cell culture expertise, Dr. Richard Kovács and Dr. Gisela Laettig for their support optimizing Ca^{2+} imaging experiments, and Smilla Maierhof for her support in cell culture maintenance and intellectual input in the final phase of the study. This research was supported by the Deutsche Forschungsgemeinschaft (NeuroCure Excellence Cluster to ME) and AnimalFreeResearch Switzerland to CS, WB and ME. This work was supported by Charité 3R - Replace - Reduce – Refine. ME receives funding from the Bundesministerium für Bildung und Forschung (Center for Stroke Research Berlin), the German Center for Neurodegenerative Diseases (DZNE), the German Center for Cardiovascular Research (DZHK) and the Corona Foundation. CS, PH and WB are members of the *Clinician Scientist* program funded by the Charité Universitätsmedizin Berlin and Berlin Institute of Health. PH is the recipient of a Rahel-Hirsch fellowship funded by the Charité Universitätsmedizin Berlin. The graphical abstract was created with BioRender.com.

Author contributions

CS, VFV, PH, WB, HS and ME designed the study. CS performed all cell culture experiments. VFV and CS performed experiments of automated microscopy. AI and DB performed computational analyses of the RNA Seq data. LN performed experiments of neuroprotection. PK contributed to the conceptualization, provided resources, and edited the manuscript. YP performed patch-clamp experiments. CS, PH and WB analyzed the data. CS, PH, WB and ME wrote the manuscript. All authors reviewed the manuscript.

References

Barpe, D.R., Rosa, D.D., Froehlich, P.E., 2010. Pharmacokinetic evaluation of doxorubicin plasma levels in normal and overweight patients with breast cancer and simulation of dose adjustment by different indexes of body mass. Eur. J. Pharm. Sci. 41 (3–4), 458–463.

Boehmerle, W., Splittgerber, U., Lazarus, M.B., McKenzie, K.M., Johnston, D.G., Austin, D.J., Ehrlich, B.E., 2006. Paclitaxel induces calcium oscillations via an inositol 1,4,5-trisphosphate receptor and neuronal calcium sensor 1-dependent mechanism. Proc. Natl. Acad. Sci. 103 (48), 18356–18361.

Boehmerle, W., Huehnchen, P., Endres, M., 2014. Neurologische Nebenwirkungen von Zytostatika. Aktuelle Neurologie 41 (01), 21–34.

Boehmerle, W., Huehnchen, P., Peruzzaro, S., Balkaya, M., Endres, M., 2015. Electrophysiological, behavioral and histological characterization of paclitaxel, cisplatin, vincristine and bortezomib-induced neuropathy in C57Bl/6 mice. Sci. Rep. 4 (1), 6370.

Bressolle, F., Jacquet, J.-M., Galtier, M., Jourdan, J., Donadio, D., Rossi, J.-F., 1992. Doxorubicin and doxorubicinol plasma concentrations and excretion in parotid saliva. Cancer Chemother. Pharmacol. 30 (3), 215–218.

Burridge, P.W., Matsa, E., Shukla, P., Lin, Z.C., Churko, J.M., Ebert, A.D., Lan, F., Diecke, S., Huber, B., Mordwinkin, N.M., et al., 2014. Chemically defined generation of human cardiomyocytes. Nat. Methods 11 (8), 855–860.

Burridge, P.W., Li, Y.F., Matsa, E., Wu, H., Ong, S.-G., Sharma, A., Holmström, A., Chang, A.C., Coronado, M.J., Ebert, A.D., et al., 2016. Human induced pluripotent stem cell–derived cardiomyocytes recapitulate the predilection of breast cancer patients to doxorubicin-induced cardiotoxicity. Nat. Med. 22 (5), 547–556.

Canet-Pons, J., Sen, N.-E., Arsović, A., Almaguer-Mederos, L.-E., Halbach, M.V., Key, J., Döring, C., Kerksiek, A., Picchiarelli, G., Cassel, R., et al., 2021. Atxn2-CAG100-KnockIn mouse spinal cord shows progressive TDP43 pathology associated with cholesterol biosynthesis suppression. Neurobiol. Dis. 152, 105289.

Cavaletti, G., Tredici, G., Marmiroli, P., Petruccioli, M.G., Barajon, I., Fabbrica, D., 1992. Morphometric study of the sensory neuron and peripheral nerve changes induced by chronic cisplatin (DDP) administration in rats. Acta Neuropathol. 84, 4.

Cermenati, G., Audano, M., Giatti, S., Carozzi, V., Porretta-Serapiglia, C., Pettinato, E., Ferri, C., D'Antonio, M., Emma, Crestani M., et al., 2015. Lack of sterol regulatory element binding factor-1c imposes glial fatty acid utilization leading to peripheral neuropathy. Cell Metab. 21 (4), 571–583.

Chambers, S.M., Qi, Y., Mica, Y., Lee, G., Zhang, X.-J., Niu, L., Bilsland, J., Cao, L., Stevens, E., Whiting, P., et al., 2012. Combined small-molecule inhibition accelerates developmental timing and converts human pluripotent stem cells into nociceptors. Nat. Biotechnol. 30 (7), 715–720.

Chandrasekhar, A., Komirishetty, P., Areti, A., Krishnan, A., Zochodne, D.W., 2021. Dual specificity phosphatases support axon plasticity and viability. Mol. Neurobiol. 58 (1), 391–407.
De Jongh, F.E., Gallo, J.M., Shen, M., Verweij, J., Sparreboom, A., 2004. Population pharmacokinetics of cisplatin in adult cancer patients. Cancer Chemother. Pharmacol. 54 (2), 105–112.
Diasio, R.B., Harris, B.E., 1989. Clinical pharmacology of 5-fluorouracil. Clin. Pharmacokinet. 16 (4), 215–237.
Dobin, A., Davis, C.A., Schlesinger, F., Drenkow, J., Zaleski, C., Jha, S., Batut, P., Chaisson, M., Gingeras, T.R., 2013. STAR: ultrafast universal RNA-seq aligner. Bioinformatics 29 (1), 15–21.
Duggett, N.A., Griffiths, L.A., Flatters, S.J.L., 2017. Paclitaxel-induced painful neuropathy is associated with changes in mitochondrial bioenergetics, glycolysis, and an energy deficit in dorsal root ganglia neurons. Pain 158 (8), 1499–1508.
Edgar, R., 2002. Gene expression omnibus: NCBI gene expression and hybridization array data repository. Nucleic Acids Res. 30 (1), 207–210.
Eldridge, S., Guo, L., Hamre, J., 2020. A comparative review of chemotherapy-induced peripheral neuropathy in in vivo and in vitro models. Toxicol. Pathol. 48 (1), 190–201.
Feinberg, K., Kolaj, A., Wu, C., Grinshtein, N., Krieger, J.R., Moran, M.F., Rubin, L.L., Miller, F.D., Kaplan, D.R., 2017. A neuroprotective agent that inactivates prodegenerative TrkA and preserves mitochondria. J. Cell Biol. 216 (11), 3655–3675.
Fusaki, N., Ban, H., Nishiyama, A., Saeki, K., Hasegawa, M., 2009. Efficient induction of transgene-free human pluripotent stem cells using a vector based on Sendai virus, an RNA virus that does not integrate into the host genome. Proc. Jpn. Acad. Ser. B 85 (8), 348–362.
Goodrum, J.F., Brown, J.C., Fowler, K.A., Bouldin, T.W., 2000. Axonal regeneration, but not myelination, is partially dependent on local cholesterol reutilization in regenerating nerve. J. Neuropathol. Exp. Neurol. 59 (11), 1002–1010.
Gu, H., Wang, C., Li, J., Yang, Y., Sun, W., Jiang, C., Li, Y., Ni, M., Liu, W.T., Cheng, Z., et al., 2020. High mobility group box-1-toll-like receptor 4-phosphatidylinositol 3-kinase/protein kinase B-mediated generation of matrix metalloproteinase-9 in the dorsal root ganglion promotes chemotherapy-induced peripheral neuropathy. Int. J. Cancer 146 (10), 2810–2821.
Hantke, J., Carty, L., Wagstaff, L.J., Turmaine, M., Wilton, D.K., Quintes, S., Koltzenburg, M., Baas, F., Mirsky, R., Jessen, K.R., 2014. C-Jun activation in Schwann cells protects against loss of sensory axons in inherited neuropathy. Brain J. Neurol. 137 (11), 2922–2937.
Hennig, A.F., Rössler, U., Boiti, F., Von Der Hagen, M., Gossen, M., Kornak, U., Stachelscheid, H., 2019. Generation of a human induced pluripotent stem cell line (BIHi002-A) from a patient with CLCN7-related infantile malignant autosomal recessive osteopetrosis. Stem Cell Res. 35, 101367.
Hertz, D.L., Kidwell, K.M., Vangipuram, K., Li, F., Pai, M.P., Burness, M., Griggs, J.J., Schott, A.F., Van Poznak, C., Hayes, D.F., et al., 2018. Paclitaxel plasma concentration after the first infusion predicts treatment-limiting peripheral neuropathy. Clin. Cancer Res. 24 (15), 3602–3610.
Huehnchen, P., Boehmerle, W., Springer, A., Freyer, D., Endres, M., 2017. A novel preventive therapy for paclitaxel-induced cognitive deficits: preclinical evidence from C57BL/6 mice. Transl. Psychiatry 7 (8), e1185.
Jodrell, D.I., Stewart, M., Aird, R., Knowles, G., Bowman, A., Wall, L., Cummings, J., McLean, C., 2001. 5-fluorouracil steady state pharmacokinetics and outcome in patients receiving protracted venous infusion for advanced colorectal cancer. Br. J. Cancer 84 (5), 600–603.
Kallenborn-Gerhardt, W., Lu, R., Syhr, K.M.J., Heidler, J., Von Melchner, H., Geisslinger, G., Bangsow, T., Schmidtko, A., 2013. Antioxidant activity of sestrin 2 controls neuropathic pain after peripheral nerve injury. Antioxid. Redox Signal. 19 (17), 2013–2023.
Kim, A.Y., Tang, Z., Liu, Q., Patel, K.N., Maag, D., Geng, Y., Dong, X., 2008. Pirt, a Phosphoinositide-binding protein, functions as a regulatory subunit of TRPV1. Cell 133 (3), 475–485.
Kim, S.-H., Choi, M.K., Park, N.Y., Hyun, J.-W., Lee, M.Y., Kim, H.J., Jung, S.K., Cha, Y., 2020. Serum neurofilament light chain levels as a biomarker of neuroaxonal injury and severity of oxaliplatin-induced peripheral neuropathy. Sci. Rep. 10, 1.
Knauss, S., Ginesta Roque, L., Hühnchen, P., Heinzerling, L., Böhmerle, W., Endres, M., 2019. Neurological side effects of checkpoint inhibitors. Nervenarzt 90 (2), 138–147.
Li, Y., Adamek, P., Zhang, H., Tatsui, C.E., Rhines, L.D., Mrozkova, P., Li, Q., Kosturakis, A.K., Cassidy, R.M., Harrison, D.S., et al., 2015. The Cancer chemotherapeutic paclitaxel increases human and rodent sensory neuron responses to TRPV1 by activation of TLR4. J. Neurosci. 35 (39), 13487–13500.
Li, Y., North, R.Y., Rhines, L.D., Tatsui, C.E., Rao, G., Edwards, D.D., Cassidy, R.M., Harrison, D.S., Johansson, C.A., Zhang, H., et al., 2018. DRG voltage-gated sodium channel 1.7 is upregulated in paclitaxel-induced neuropathy in rats and in humans with neuropathic pain. J. Neurosci. 38 (5), 1124–1136.
Li, Y., Marri, T., North, R.Y., Rhodes, H.R., Uhelski, M.L., Tatsui, C.E., Rhines, L.D., Rao, G., Corrales, G., Abercrombie, T.J., et al., 2021. Chemotherapy-induced peripheral neuropathy in a dish: dorsal root ganglion cells treated in vitro with paclitaxel show biochemical and physiological responses parallel to that seen in vivo. Pain 162 (1), 84–96.
Liao, Y., Smyth, G.K., Shi, W., 2014. FeatureCounts: an efficient general purpose program for assigning sequence reads to genomic features. Bioinformatics 30 (7), 923–930.
Love, M.I., Huber, W., Anders, S., 2014. Moderated estimation of fold change and dispersion for RNA-seq data with DESeq2. Genome Biol. 15, 12.
Mahmoudpour, S.H., Bandapalli, O.R., Da Silva Filho, M.I., Campo, C., Hemminki, K., Goldschmidt, H., Merz, M., Försti, A., 2018. Chemotherapy-induced peripheral neuropathy: evidence from genome-wide association studies and replication within multiple myeloma patients. BMC Cancer 18, 1.
Meents, J.E., Bressan, E., Sontag, S., Foerster, A., Hautvast, P., Rösseler, C., Hampl, M., Schüler, H., Goetzke, R., Le, T.K.C., et al., 2019. The role of Nav1.7 in human nociceptors. PAIN 160 (6), 1327–1341.
Meregalli, C., Fumagalli, G., Alberti, P., Canta, A., Chiorazzi, A., Monza, L., Pozzi, E., Carozzi, V.A., Blennow, K., Zetterberg, H., et al., 2020. Neurofilament light chain: a specific serum biomarker of axonal damage severity in rat models of chemotherapy-induced peripheral neurotoxicity. Arch. Toxicol. 94 (7), 2517–2522.
Mo, M., Erdelyi, I., Szigeti-Buck, K., Benbow, J.H., Ehrlich, B.E., 2012. Prevention of paclitaxel-induced peripheral neuropathy by lithium pretreatment. FASEB J. 26 (11), 4696–4709.
Moreau, P., Pylypenko, H., Grosicki, S., Karamanesht, I., Leleu, X., Grishunina, M., Rekhtman, G., Masliak, Z., Robak, T., Shubina, A., et al., 2011. Subcutaneous versus intravenous administration of bortezomib in patients with relapsed multiple myeloma: a randomised, phase 3, non-inferiority study. Lancet Oncol. 12 (5), 431–440.
Muke, I., Sprenger, A., Bobylev, I., Wiemer, V., Barham, M., Neiss, W.F., Lehmann, H.C., 2020. Ultrastructural characterization of mitochondrial damage in experimental autoimmune neuritis. J. Neuroimmunol. 343, 577218.
Namer, B., Schmidt, D., Eberhardt, E., Maroni, M., Dorfmeister, E., Kleggetveit, I.P., Kaluza, L., Meents, J., Gerlach, A., Lin, Z., et al., 2019. Pain relief in a neuropathy patient by lacosamide: proof of principle of clinical translation from patient-specific iPS cell-derived nociceptors. EBioMedicine 39, 401–408.
Nelson, R.L., 1982. The comparative clinical pharmacology and pharmacokinetics of vindesine, vincristine, and vinblastine in human patients with cancer. Med. Pediatr. Oncol. 10 (2), 115–127.
Omura, T., Omura, K., Tedeschi, A., Riva, P., Michio Rojas, L., Martin, J., Lisi, V., Eric Latremoliere, A., et al., 2015. Robust axonal regeneration occurs in the injured CAST/Ei mouse CNS. Neuron 86 (5), 1215–1227.
Peng, Y., Barreda Tomas, F.J., Klisch, C., Vida, I., Geiger, J.R.P., 2017. Layer-specific organization of local excitatory and inhibitory synaptic connectivity in the rat presubiculum. Cereb. Cortex 27 (4), 2435–2452.
Peng, Y., Mittermaier, F.X., Planert, H., Schneider, U.C., Alle, H., Geiger, J.R.P., 2019. High-throughput microcircuit analysis of individual human brains through next-generation multineuron patch-clamp. eLife 8.
Pereira, A.F., Pereira, L.M.S., Silva, C.M.P., Freitas Alves, B.W., Barbosa, J.S., Pinto, F.M. M., Pereira, A.C., Silva, K.O., Pontes, R.B., Alencar, N.M.N., et al., 2019. Metformin reduces c-Fos and ATF3 expression in the dorsal root ganglia and protects against oxaliplatin-induced peripheral sensory neuropathy in mice. Neurosci. Lett. 709, 134378.
Pittman, S.K., Gracias, N.G., Vasko, M.R., Fehrenbacher, J.C., 2014. Paclitaxel alters the evoked release of calcitonin gene-related peptide from rat sensory neurons in culture. Exp. Neurol. 253, 146–153.
Rajkumar, P., Mathew, B.S., Das, S., Isaiah, R., John, S., Prabha, R., Fleming, D.H., 2016. Cisplatin concentrations in long and short duration infusion: implications for the optimal time of radiation delivery. J. Clin. Diagn. Res. 10 (7), Xc01–Xc04.
Reece, D.E., Sullivan, D., Lonial, S., Mohrbacher, A.F., Chatta, G., Shustik, C., Burris, H., Venkatakrishnan, K., Neuwirth, R., Riordan, W.J., et al., 2011. Pharmacokinetic and pharmacodynamic study of two doses of bortezomib in patients with relapsed multiple myeloma. Cancer Chemother. Pharmacol. 67 (1), 57–67.
Rostock, C., Schrenk-Siemens, K., Pohle, J., Siemens, J., 2018. Human vs. mouse nociceptors – Similarities and differences. Neuroscience 387, 13–27.
Rowinsky, E.K., Donehower, R.C., 1995. Paclitaxel steady-state plasma concentration as a determinant of disease outcome and toxicity in lung Cancer patients treated with paclitaxel and cisplatin. N. Engl. J. Med. 332 (15), 1004–1014.
Röytta, M., Raine, C.S., 1985. Taxol-induced neuropathy: further ultrastructural studies of nerve fibre changesin situ. J. Neurocytol. 14 (1), 157–175.
Sanchez, J.C., Munoz, L.V., Ehrlich, B.E., 2020. Modulating TRPV4 channels with paclitaxel and lithium. Cell Calcium 91, 102266.
Schoepf, C.L., Zeidler, M., Spiecker, L., Kern, G., Lechner, J., Kummer, K.K., Kress, M., 2020. Selected ionotropic receptors and voltage-gated ion channels: more functional competence for human induced pluripotent stem cell (iPSC)-derived nociceptors. Brain Sci. 10 (6), 344.
Schwartz, R., Davidson, T., 2004. Pharmacology, pharmacokinetics, and practical applications of bortezomib. Oncology (Williston Park) 18 (14 Suppl 11), 14–21.
Schwartzentruber, J., Foskolou, S., Kilpinen, H., Rodrigues, J., Alasoo, K., Knights, A.J., Patel, M., Goncalves, A., Ferreira, R., Benn, C.L., et al., 2018. Molecular and functional variation in iPSC-derived sensory neurons. Nat. Genet. 50 (1), 54–61.
Sebbagh, M., Renvoizé, C., Hamelin, J., Riché, N., Bertoglio, J., Bréard, J., 2001. Caspase-3-mediated cleavage of ROCK I induces MLC phosphorylation and apoptotic membrane blebbing. Nat. Cell Biol. 3 (4), 346–352.
Seijffers, R., Mills, C.D., Woolf, C.J., 2007. ATF3 increases the intrinsic growth state of DRG neurons to enhance peripheral nerve regeneration. J. Neurosci. 27 (30), 7911–7920.
Seretny, M., Currie, G.L., Sena, E.S., Ramnarine, S., Grant, R., Macleod, M.R., Colvin, L. A., Fallon, M., 2014. Incidence, prevalence, and predictors of chemotherapy-induced peripheral neuropathy: a systematic review and meta-analysis. Pain 155 (12), 2461–2470.
Smith, E.M.L., Pang, H., Cirrincione, C., Fleishman, S., Paskett, E.D., Ahles, T., Bressler, L.R., Fadul, C.E., Knox, C., Le-Lindqwister, N., et al., 2013. Effect of duloxetine on pain, function, and quality of life among patients with chemotherapy-induced painful peripheral neuropathy. JAMA 309 (13), 1359.
Spicarova, D., Nerandzic, V., Palecek, J., 2011. Modulation of spinal cord synaptic activity by tumor necrosis factor α in a model of peripheral neuropathy. J. Neuroinflammation 8 (1), 177.

Sproule, B., 2002. Lithium in bipolar disorder. Clin. Pharmacokinet. 41 (9), 639–660.
Stacey, P., Wassermann, A.M., Kammonen, L., Impey, E., Wilbrey, A., Cawkill, D., 2018. Plate-based phenotypic screening for pain using human iPSC-derived sensory neurons. SLAS DISCOVERY: Adv. Life Sci. R&D 23 (6), 585–596.
Stelzer, G., Rosen, N., Plaschkes, I., Zimmerman, S., Twik, M., Fishilevich, S., Stein, T.I., Nudel, R., Lieder, I., Mazor, Y., et al., 2016. The GeneCards suite: from gene data mining to disease genome sequence analyses. Curr. Protoc. Bioinformatics 54 (1), 30 31–31 30 33.
Syc-Mazurek, S.B., Fernandes, K.A., Wilson, M.P., Shrager, P., Libby, R.T., 2017. Together JUN and DDIT3 (CHOP) control retinal ganglion cell death after axonal injury. Mol. Neurodegener. 12, 1.
Takahashi, K., Tanabe, K., Ohnuki, M., Narita, M., Ichisaka, T., Tomoda, K., Yamanaka, S., 2007. Induction of pluripotent stem cells from adult human fibroblasts by defined factors. Cell 131 (5), 861–872.
Urien, S., Lokiec, F., 2004. Population pharmacokinetics of total and unbound plasma cisplatin in adult patients. Br. J. Clin. Pharmacol. 57 (6), 756–763.
Van Den Berg, H.W., Desai, Z.R., Wilson, R., Kennedy, G., Bridges, J.M., Shanks, R.G., 1982. The pharmacokinetics of vincristine in man. Cancer Chemother. Pharmacol. 8 (2), 215–219.
Vermorken, J.B., van der Vijgh, W.J., Klein, I., Hart, A.A., Gall, H.E., Pinedo, H.M., 1984. Pharmacokinetics of free and total platinum species after short-term infusion of cisplatin. Cancer Treat. Rep. 68 (3), 505–513.
Vojnits, K., Mahammad, S., Collins, T.J., Bhatia, M., 2019. Chemotherapy-induced neuropathy and drug discovery platform using human sensory neurons converted directly from adult peripheral blood. Stem Cells Transl. Med. 8 (11), 1180–1191.
Von Der Ahe, D., Huehnchen, P., Balkaya, M., Peruzzaro, S., Endres, M., Boehmerle, W., 2018. Suramin-induced neurotoxicity: preclinical models and neuroprotective strategies. Molecules (Basel, Switzerland) 23 (2), 346.
Walle, T., Walle, U.K., Kumar, G.N., Bhalla, K.N., 1995. Taxol metabolism and disposition in cancer patients. Drug Metab. Dispos. 23 (4), 506–512.
Wang, J.T., Medress, Z.A., Barres, B.A., 2012. Axon degeneration: molecular mechanisms of a self-destruction pathway. J. Cell Biol. 196 (1), 7–18.
Wangzhou, A., Paige, C., Neerukonda, S.V., Naik, D.K., Kume, M., David, E.T., Dussor, G., Ray, P.R., Price, T.J., 2021. A ligand-receptor interactome platform for discovery of pain mechanisms and therapeutic targets. Sci. Signal. 14 (674), eabe1648.
Wheeler, H.E., Wing, C., Delaney, S.M., Komatsu, M., Dolan, M.E., 2015. Modeling chemotherapeutic neurotoxicity with human induced pluripotent stem cell-derived neuronal cells. PLoS One 10 (2), e0118020.
Wing, C., Komatsu, M., Delaney, S.M., Krause, M., Wheeler, H.E., Dolan, M.E., 2017. Application of stem cell derived neuronal cells to evaluate neurotoxic chemotherapy. Stem Cell Res. 22, 79–88.
Xiong, C., Chua, K.C., Stage, T.B., Priotti, J., Kim, J., Altman-Merino, A., Chan, D., Saraf, K., Canato Ferracini, A., Fattahi, F., et al., 2021. Human induced pluripotent stem cell derived sensory neurons are sensitive to the neurotoxic effects of paclitaxel. Clin. Transl. Sci. 14 (2), 568–581. https://doi.org/10.1111/cts.12912.
Yamada, Y., Hamaguchi, T., Goto, M., Muro, K., Matsumura, Y., Shimada, Y., Shirao, K., Nagayama, S., 2003. Plasma concentrations of 5-fluorouracil and F-β-alanine following oral administration of S-1, a dihydropyrimidine dehydrogenase inhibitory fluoropyrimidine, as compared with protracted venous infusion of 5-fluorouracil. Br. J. Cancer 89 (5), 816–820.
Yan, Z., Zhu, Z.-L., Qian, Z.-Z., Hu, G., Wang, H.-Q., Liu, W.-H., Cheng, G., 2012. Pharmacokinetic characteristics of vincristine sulfate liposomes in patients with advanced solid tumors. Acta Pharmacol. Sin. 33 (6), 852–858.
Yang, F., Jiang, M., Lu, M., Hu, P., Wang, H., Jiang, J., 2018. Pharmacokinetic behavior of vincristine and safety following intravenous administration of vincristine sulfate liposome injection in Chinese patients with malignant lymphoma. Front. Pharmacol. 9.
Zhang, J.-H., Chung, T.D.Y., Oldenburg, K.R., 1999. A simple statistical parameter for use in evaluation and validation of high throughput screening assays. J. Biomol. Screen. 4 (2), 67–73.
Zyla, J., Marczyk, M., Domaszewska, T., Kaufmann, S.H.E., Polanska, J., Weiner, J., 2019. Gene set enrichment for reproducible science: comparison of CERNO and eight other algorithms. Bioinformatics 35 (24), 5146–5154.